

**NOVEL APPLICATIONS OF FLOW CYTOMETRY TO
ASSESS WHOLE MURINE SKELETAL MUSCLE AND
MYONUCLEI NUMBER RESPONSES TO ATROPHY
AND RECOVERY.**

MARK ROBERT VIGGARS

**A thesis submitted in partial fulfilment of the requirements of
Liverpool John Moores University for the degree of Master of
Philosophy**

September 2018

Student:

**Mark Viggars (BSc Hons, AFHEA),
Research Institute for Sport and Exercise Sciences (RISES),
Liverpool John Moores University,
Liverpool,
L3 3AF,
United Kingdom**

Director of Studies:

**Jonathan Jarvis BSc PhD DIC ARCS FHEA
Professor of Sport and Exercise Science
Research Institute for Sport & Exercise Sciences (RISES),
Liverpool John Moores University,
Liverpool,
L3 3AF
United Kingdom**

Summary

This thesis will present an introduction to cellular and molecular adaptation to loading and unloading of skeletal muscle, whilst exploring the advantages and disadvantages of current techniques employed in the field of exercise biochemistry. In response to the current techniques used to assess the signal transduction and protein changes present in response to loading and unloading, we propose a potential, novel method of assessing whole, murine skeletal muscle protein isoforms via flow cytometry. In addition to this, this thesis also explores the changes in morphology and myonuclear number within skeletal muscle following varying periods of atrophy, and recovery from atrophy produced in response to tetrodotoxin administration to silence a motor nerve and therefore muscular contraction in the ankle dorsiflexor muscles of the rat hindlimb.

Contents	Page
Summary	2
Chapter 1: An introduction to skeletal muscle adaptation to loading and unloading.	4
Chapter 2: A critical overview of methods used in exercise biochemistry.	9
Chapter 3: <i>Study 1</i> : Optimisation of whole murine skeletal muscle fiber dispersion for use in flow cytometry.	15
Chapter 3: <i>Study 2</i> : Assessment of fiber size and type via flow cytometry using whole murine skeletal muscles.	21
Chapter 4: Nuclear Density in muscle atrophy/injury and recovery from atrophy/injury.	32
Chapter 6: Future Directions for PhD study	54
References	56

Chapter 1: An introduction to skeletal muscle adaptation to loading and unloading.

Hypertrophy Signalling Pathways

Chronic strength training brings about adaptive responses that allow skeletal muscle to meet the demands of future bouts of resistance training. Typically, this results in increased muscular hypertrophy (an accumulation of myofibrillar proteins, subsequently increasing muscle cross sectional area) and strength, if protein synthesis increases to a greater extent and duration than degradation (Phillips, 2014; Wackerhage & Ratkevicius, 2008). Armstrong *et al.*, (1993) in rodents and Roth *et al.*, (1999) in humans reported that performing eccentric strength training caused localised disruption of normal myofibrillar banding patterns. For the myofibril to reconstitute its functional contractile state and adapt to future bouts of resistance, myofilaments must be repaired or replaced as the body continually turns over proteins in a state of positive net protein balance (Phillips, 2014; Yin *et al.*, 2013). This remodelling process can alter dependent on whether the muscle is eccentrically or concentrically loaded (Franchi *et al.*, 2017). However, it seems that both eccentric and concentric loading follow the same mechanotransduction pathway in order to activate the anabolic mTOR signal transduction pathway to increase protein synthesis, thus levels of hypertrophy are generally found to be the same between contraction types, if total volume of load is the same (Franchi *et al.*, 2017), despite the large variance in loading experienced between eccentric, concentric and co-contraction models (Schmoll *et al.*, 2017). The only resultant difference in remodelling following these different contraction states may be where new protein is laid down (eccentric- in series, concentric- moreso in parallel), the actual protein content and remodelling of the extra-cellular matrix/stem cell niche, as opposed to changes in total protein content (Franchi *et al.*, 2017; Hyldahl *et al.*, 2015; Jakobsen *et al.*, 2018).

Since its discovery in the early 1990's by Schreiber & Sabatini (Brown *et al.*, 1994; Sabatini *et al.*, 1994), mechanistic target of rapamycin (mTOR) has been recognised as the key nutrient, energy and redox status sensor within eukaryotic cells responsible for controlling protein synthesis. mTOR itself exists in two protein complexes; mTORC1 and mTORC2 which are associated with different locations within a cell and phosphorylation of different proteins. In relation to resistance exercise, Baar and Esser, (1999) identified that mTORC1 signalling cascade was activated by electrically stimulated, resistance exercise in a rodent model. mTORC1 can directly phosphorylate S6K1 on a hydrophobic motif site, Thr389 allowing for phosphorylation and activation by PDK1; the activation of which promotes ribosomal biogenesis, mRNA translation initiation and also phosphorylates 4EBP which results in increased translation efficiency (Saxton & Sabatini, 2017), The amount of p70s6k phosphorylation was found to be directly related to the degree of hypertrophy (Baar and Esser, 1999).

The actual pathway responsible for the signal transduction of mechanical stimuli to a biochemical signal, termed mechanotransduction is still not largely understood due to an unidentified mechanoreceptor which inhibits tuberous sclerosis complex 2 (TSC2), resulting in the activation of Rheb and mTOR. Research by the Hornberger group has illustrated that this mechanically stimulated increase in mTOR activation may occur through a mechanism that requires phosphatidic acid and a phosphatidic acid synthesising enzyme called diacylglycerol kinase zeta (DGK ζ) (Hornberger *et al.*, 2006). Muscles deficient in the DGK ζ enzyme have a reduced capacity to activate mTOR by up to 50% (You *et al.*, 2014; You *et al.*, 2018). Protein co-localisation studies have revealed that following resistance exercise, mTOR co-localises with late endosomal-lysosomal system (Jacobs *et al.*, 2013), that have recently been reported to contain high levels of phosphatidic acid and Rheb (Zhang *et al.*, 2013). Furthermore, prior to resistance exercise Rheb's ability to activate mTOR is inhibited by TSC2 and TSC2 is found to be co-localised with Rheb. Following resistance exercise, this association with TSC2 with the LEL is removed, therefore allowing for activation of mTOR (Jacobs *et al.*, 2013; Jacobs *et al.*, 2017; Sawan *et al.*, 2018; Song *et al.*, 2017). With advancements in proteomics and phosphoproteomics, it is expected that this mechanotransduction pathway will continue to be uncovered (Potts *et al.*, 2017).

However, the degree to which muscle hypertrophies may also be interrupted through the molecular responses present when resistance exercise is combined with endurance exercise. Specifically through elevated AMP levels and AMPK phosphorylation levels which have previously been negatively correlated with skeletal muscle hypertrophy and protein synthesis after acute bouts of concurrent training (Bodine *et al.*, 2001; Bolster *et al.*, 2002; Katta *et al.*, 2012; Thomson *et al.*, 2008). Genetic knockout of AMPK results in greater hypertrophy (Mounier *et al.*, 2009), by preventing direct phosphorylation of TSC2, thus preventing Rheb's activation of mTOR and downstream cascade of protein translation and synthesis (Inoki *et al.*, 2002). This mechanism may be to potentially prevent muscle protein synthesis and growth when energy is required elsewhere.

Hyperplasia

A less common phenomenon found within human physiology of increasing muscle size is termed 'hyperplasia', the increase in number of individual muscle fibres. Whilst numerous animal models have previously shown that supra-physiological loading, synergist ablation and denervation can result in an increase in number of fibres and/or cause fiber branching or splitting in an overloaded muscle (Antonio & Gonyea, 1993, 1994; Ho *et al.*, 1980; Tamaki *et al.*, 1992), the mechanisms and exact stimulus resulting in this are yet to be elucidated. This is in part due to the following methodological issues: 1; Histological analysis is often constrained to a biopsy sample of a muscle, and therefore may not be representative of the whole muscle

due to the huge variations in fiber architecture and composition of fiber types across different heads of multipennate muscles, 2; The phenomenon of fibre splitting would convey a false increase in fibre number when assessed via histological cross-sections. However, if fibre bundles from skeletal muscle were separated into individual myofibers using gentle collagenase treatment, it would be observed that fibers actually split and branch out as opposed to becoming a completely new muscle fiber (Antonio & Gonyea, 1993, 1994). Whilst under certain conditions of mechanical stretch and overload skeletal muscle hyperplasia has been shown to occur, albeit mostly in animal models, the mechanisms behind this have yet to be explored and have seemingly received very little recent attention in the field of skeletal muscle adaptation. This may be due to the fact that the only way of truly establishing whether hyperplasia has occurred is by assessing the number of fibres across the whole muscle as opposed to a biopsy and to extract the tissue at a timepoint where this occurs. Whilst this is clearly not possible in humans, advancements in in-vivo imaging techniques with animal models (Bruusgaard & Gundersen, 2008), may one day make the investigation into the exact stimulus and process possible.

Satellite cells and their contribution to muscle regeneration

Skeletal muscle repair following eccentric damage is a complex mechanism attributed not only to the balance of protein synthesis and degradation, but also involves the confluence of both the activation and differentiation of satellite cells-specific to muscular lineage, adding additional myonuclei to existing myotubes or if the stress is severe enough causing formation of 'de novo' myofibers by satellite cells fusing together; producing hypertrophy (Knapp *et al.*, 2015). Satellite cells are mononucleated, multipotent, myogenic pre-cursor cells and are the local source of repair, regeneration and growth following myofibrillar damage in post-natal mammals, ensuring that mechanical, structural and functional integrity of skeletal muscle is maintained following exercise or injury (Hawke and Garry, 2001).

Satellite cells represent the primary pool of stem cells resident within adult skeletal muscle and are responsible for both muscle fibre repair and generation of new myofibers (hyperplasia); both of which contribute to hypertrophy. Satellite cells located in a quiescent state beneath the basal lamina of the myofiber, have the capacity once activated to proliferate, differentiate and fuse to damaged myofibers to carry out regeneration/repair of muscle tissue and for hypertrophy to occur following resistance training (Hawke and Garry, 2001). Despite the paucity of satellite cells associated with an individual myofiber, making up just 2.5-6% of fiber nuclei, they can be rapidly activated to restore exercise-induced damage (Zammit *et al.*, 2004). Specifically, the processes following exercise-induced muscle damage are brought about by a family of proteins known as myogenic regulatory factors (MRF) (Nederveen *et al.*,

2017). Firstly, to become activated following exercise or damage, a cascade of cell signaling occurs bringing about the release of growth factors such as HGF, MGF, IGF-I and FGF2 which then bind to receptors present on the quiescent satellite cell, thus activating it (Hill *et al.*, 2003a; Pelosi *et al.*, 2007). Activated satellite cells initially express two MRFs, myogenic differentiation factor (MyoD1) and Myogenic factor 5 (Grobler *et al.*, 2004); which are expressed at extremely low levels during quiescence (Rudnicki *et al.*, 1993). From this point, satellite cells can proliferate via upregulation of the transcription factor paired box protein 7 (Pax7), without which satellite cell lineage would be lost (Von Maltzahn *et al.*, 2013), or return to a state of quiescence where MyoD1 will be downregulated and the population of satellite cells restored (Baumert *et al.*, 2016).

Alternatively, when tasked to repair damaged myofibers, satellite cells withdraw from the cell cycle and differentiate, accompanied by the upregulation of herculin and myogenin (Arnold and Braun, 2003; Miner and Wold, (1990). Myoblasts differentiate into myocytes which migrate along chemotactic gradients to the injured myofibers and support the repair by increasing the number of active myonuclei of existing fibres and thus, providing support to the larger cytoplasmic volume (Egner *et al.*, 2016). However, if the extent of damage is too large to repair or involves the destruction and removal of the existing fibres via macrophages, the differentiated myocytes fuse with other myogenic cells forming myotubes, producing new 'de novo' myofibers replacing the damaged fibres (Tidball, 2011).

Processes such as ageing, dystrophies and physical inactivity have a negative impact on skeletal muscle repair due to the significant reduction in regenerative capacity; attributed to the decreased ability of satellite cells to proliferate, occurring in adulthood and declining further still in the elderly populations. Much of the loss in proliferative ability in adulthood and the switch to reliance on remodeling and hypertrophy of existing fibres is due to the long lifespan of satellite cells, therefore making satellite cells vulnerable to accumulation of cellular damage, causing a reduction in their capability to self-renew, as well as the whole muscle itself. The eventual outcome of this is reduction in the satellite cell pool and debilitating changes in their resident microenvironment, therefore delaying or reducing capability of skeletal muscle repair following exercise or severe injury. (Billin *et al.*, 2016; Chandel *et al.*, 2016; Fehrer and Lepperdinger, 2005). However, the significant loss of muscle mass, strength and quality of life associated with skeletal muscle ageing (sarcopenia) can be reduced through appropriate nutrition and hormonal adaptations to exercise (Morley *et al.*, 2010). Current recommendations to promote healthy ageing include resistance and aerobic exercise, combined with a leucine-rich protein diet; both of which are key in upregulating mTOR signal transduction pathways which increase protein synthesis and activating satellite cell pathways

which aid in acute repair of damaged myofibers and long-term hypertrophy (Campbell and Leidy 2007; Johnston *et al.*, 2007). Therefore, developing a better understanding of the proliferative capacity and differentiation of satellite cells following different stimulation patterns will help designate appropriate intervention for repair of injured muscle and reduction in disease-related or ageing muscle wastage. Alongside this, there is the potential to identify specific training patterns that avoid excessive 'endurance like' stimuli, or even 'overtraining' in which damage occurs rather than repair, amplifying hypertrophy for both sports performance and the increasing ageing population (Johnston *et al.*, 2007).

Although Lepper *et al.*, (2011) confirming that elimination of Pax7⁺ cells through genetic ablation completely blocks regeneration of any myofibers following acute injury in mice, fully functional, regenerative myogenesis requires the interaction of multiple cell types including fibroblasts, not surprisingly due to the abundance of connective tissue fibrosis often occurring around the site of severe myofiber injury (Mackey *et al.*, 2017). Understanding these myogenic-fibroblast interactions is essential to help prevent impaired healing, especially in the elderly who characteristically have a higher abundance of fibroblasts, which subsequently replace contractile proteins with fibrous/fatty scar tissue, resulting in loss of strength and an increased risk of falling and frailty (Maddaluno *et al.*, 2017; Morley *et al.*, 2010).

In-vivo studies from Murphy *et al.*, (2011), utilizing a mouse model whereby genetic insertion allows targeted destruction of Pax7⁺ and Tcf4 cells, through tamoxifen injection which activates Cre, which subsequently activates diphtheria toxin A ablating Pax7⁺ and Tcf4 cells. Injury following the ablation of satellite cells causes misregulation of Tcf4 fibroblasts to the extent that expansion of fibroblasts was reduced by 52%. Contrastingly, ablation of Tcf4 fibroblasts caused a 51% reduction in Pax7 satellite cells 5 days post injury coupled with a 79% reduction in MyoD⁺ Pax7 satellite cells, indicating a large decrease in differentiating myoblasts. Partial ablation of Tcf4 fibroblasts results in premature differentiation of satellite cells to myoblasts giving rise to smaller regenerated myofibers post injury. Mathew *et al.*, (2011) also demonstrated the significance of reciprocal interactions connective tissue fibroblasts and satellite cells have in a fibroblast/myoblast trans-well culture. Cultured myoblasts alone differentiated into multinucleate myofibers, however with the addition of fibroblasts in the same culture, myotube fusion index significantly increased ($p < 0.0001$, 10 vs. 40 with fibroblasts). Mackey *et al.*, (2017) also produced electrically stimulated eccentric damage in humans and showed that there was a clear preferential association of fibroblasts with regenerating myofibers and new myofibers with central nuclei, in comparison to undamaged myofibers; with 104 ± 6.23 fibroblasts per mm^2 after injury and 26 ± 3.14 fibroblasts per mm^2 in the uninjured limb. Whilst the interactions between satellite cells,

fibroblasts and the extracellular matrix are still being understood, as well as mechanotransduction pathways, it is clear that in reality, maintenance/growth of healthy muscle mass is controlled by a complex combination and interaction of the anabolic mTOR signaling pathway and satellite cell interactions which are yet to be elucidated.

Chapter 2: An overview of methods used in exercise biochemistry.

As outlined in the first chapter, exercise biochemistry is the study of the signal transduction mechanisms that lead to adaptation to exercise, whether it be hypertrophy following resistance training or mitochondrial associated protein changes following endurance training. Whilst measurement of adaptations to exercise have long been possible at the whole-body/organ level using non-invasive methods, the understanding of adaptation to exercise has been vastly improved due to the development of the muscle biopsy technique (Bergström & Hultman, 1966), and use of biochemical methods in the past 30 years. This chapter aims to give a brief introduction into current biochemical techniques employed specifically by exercise biochemists, their applications and limitations of their use.

RT-qPCR

The polymerase chain reaction (PCR) was introduced by Kary Mullis in the 1980's to amplify small DNA fragments in order to appropriately sequence it (Mullis, 1990). This has enabled genetic association studies and genome-wide association studies to link gene polymorphisms to abnormal expression of a gene or production of an irregular form of a protein. These abnormalities can be linked to disease and injury such as COL5A1 and its link to irregular extracellular matrix formation and increased risk of non-contact ligament injury (Posthumus *et al.*, 2009; Zoppie *et al.*, 2004). However, particular polymorphisms can be linked to good health and performance, such as the ACTN3 R577X genotype association with greater power in elite-level athletes and greater hypertrophic responses to resistance exercise (Clarkson *et al.*, 2005; Yang *et al.*, 2003).

The technique has been further extended to measurement of gene expression through amplification and measurement of RNA (cDNA), therefore providing a method of understanding the signalling responses and cascades to various different exercise stimuli and nutrition that ultimately lead to adaptation. This method relies on the extraction and isolation of RNA, most popularly achieved through homogenisation of tissue combined with the reagent Trizol that contains phenol, chloroform and guanidinium thiocyanate. This solution allows tissue to become soluble, disrupting and dissolving cell components whilst effectively inhibiting RNase activity. Centrifugation of the Trizol treated homogenate results in separation into a

clear, upper aqueous layer which contains RNA, an interphase layer containing DNA and an organic phase containing proteins and lipids (Chomczynski & Sacchi, 1987). A solution containing only RNA can then be collected, washed with alcohol and the precipitate collected following centrifugation. RNA can then be quantified using spectrophotometry and is then usually converted to cDNA through reverse transcription and a reverse transcriptase enzyme.

The specific cDNA is then amplified by a polymerase chain reaction consisting of 25-35 cycles of denaturation, annealing and extension using specific primers (short strands of RNA) designed to match specific genes of interest. During the thermal cycling of the PCR, a fluorescent reporter molecule/probe is measured using a fluorimeter and increases as the product accumulates through each amplification cycle. This quantitation of a transcript is then reported relative to changes in a reference gene (a gene that's expression will not change between experimental conditions), therefore providing a semi-quantitative report of a genes expression (Wackerhage, 2014).

Whilst gene expression (RNA present within the tissue of interest) can give us an understanding of the signals being transduced following a particular stimulus, e.g. load, the upregulation or downregulation of gene expression does not always lead to changes at the protein level. This is due to a number of factors including amino acid availability, post-translational modifications and transcriptomic/epi-transcriptomic regulation of mRNA (Davalos *et al.*, 2018; Wackerhage, 2014). Whilst this technique is important to elucidate mechanisms through which resistance/endurance training controls the expression of a gene, gene expression should not be used to conclude that a change in mRNA leads to a protein change and instead, should ideally be combined with data of the amount of a protein present after exercise/nutritional intervention as suggested by Miller *et al.*, (2016).

Western Blotting

Western blotting, also known as immunoblotting is a process whereby proteins are separated in an electrical field and then detected and quantified (abundance) using specific antibodies for an antigen found on the protein of interest. As most signalling transduction is done by proteins and often involves post-translational modifications such as phosphorylation of proteins, western blotting provides a useful tool to investigate protein abundance and their modification in response to a specific stimulus (Bass *et al.*, 2017). Similarly to RT-qPCR, western blotting is a semi-quantitative assay as the abundance of a protein is always measured relative to a reference protein such as GAPDH or to expression in another control tissue. The process of western blotting first requires the extraction of protein from the tissue being investigated, usually achieved through homogenisation and treatment with Triton X-100, used as a detergent to lyse cells and release protein. The protein concentration in the resultant

supernatant is then quantified using a Bradford or Bicinchoninic acid assay (BCA) allowing for samples to be standardised to the same protein concentration. The supernatant is further treated with Laemmli buffer (Laemmli, 1970) in order to denature and negatively charge proteins with the anionic detergent sodium dodecyl sulfate (SDS). Samples are further heat denatured whilst in this solution at 95°C for 5 minutes allowing proteins to completely unfold whilst SDS binds with proteins preventing refolding of the protein when the supernatant is cooled (Bass *et al.*, 2017). Proteins can then be separated using gel electrophoresis, a process whereby proteins are equally loaded into lanes within a gel and are pulled towards a positive electrode. The smaller the protein the faster it will travel through the gel therefore ordering proteins based on their atomic mass.

These proteins can then be transferred to a nitrocellulose membrane where they can be probed at the correct molecular weight with a primary antibody that will bind selectively to a protein of interest. A secondary antibody then binds to the primary antibody and is conjugated to a fluorophore or enzyme (e.g. HRP) for visualization with a fluorometer or for the latter, a chemiluminescent camera that can capture light over a period of time from a light-emitting reaction to create a digital image. Images can then be quantified using computer software based on peak area or height of the antigen-antibody complex.

Unfortunately, there are a number of potential problems with the repeatability, accuracy and time taken to complete this method due to the nature of having to complete multiple steps as well as loading an equal amount of total protein in each well. As well as loading equal amounts of each sample into the gels, it is common practice to normalise the protein of interest relative to reference protein such as GAPDH and β -actin or total amount of protein. Even using this method, co-efficient of variation for western blotting can be between 30-50% depending on whether a high-abundance reference protein is used, or a total protein stain is used to normalise the data (Aldridge *et al.*, 2008). Producing accurate data for a large number of samples is therefore extremely difficult and there is a large body of evidence supported by the Office of Research Integrity (ORI) in the United States that laboratories have been publishing fraudulent and digitally manipulated western blots for a number of years, even producing guidelines set to expose and ensure against such misleading data (Newman, 2013).

Alternative technologies are becoming more prevalent within biochemistry to measure an individual proteins abundance and modification such as enzyme-linked immunosorbent assay (ELISA), but are significantly more expensive and are not able to be stripped and re-probed like Western Blotting. Despite this ELISA's have the advantage of analysing more samples at once (usually within a 96-well plate). Additionally, immunoassay array kits are becoming more prevalent to perform multiplex assessments of individual proteins abundance and modifications but the range of molecular targets available in this format are less diverse and less accurate in comparison to antibodies available for western blotting and

immunohistochemistry. Currently, commercially available kits are limited to cardiac, endocrine and cerebral disease assessment and have not yet been developed specifically for exercise biochemistry use.

There is also a growing interest in the application of mass spectrometry in exercise and muscle biochemistry which gives the advantage of being able to assess multiple individual protein isoforms with a high degree of sensitivity over a wide dynamic range, 0.5-500ng/μl, (Bass *et al.*, 2017). Using novel deuterium labelling, synthesis rates, abundance and degradation rates of specific proteins can also be calculated over time in response to an exercise stimulus (Brook *et al.*, 2015; Brook *et al.*, 2017; Camera *et al.*, 2017; Hesketh *et al.*, 2016; Srisawat *et al.*, 2017).

However, this analysis can be expensive and requires a relatively high level of training and technical equipment that have not yet become common place within exercise/muscle biochemistry labs.

Immunohistochemistry and immunocytochemistry

As well as being able to quantify the abundance of an individual protein and post-translational modification of the protein using western blotting, it is important to understand that these values are representative of a homogenate which may contain multiple cell types. To properly understand adaptive mechanisms to exercise, immunohistochemistry can be employed to identify where in the muscle a protein is abundant, where the post-translational modifications are occurring within the cells and whether these proteins are co-localised with each other, indicating the transduction of a biochemical signal within a cell (protein-protein interaction), for example the relationship between mTOR, TSC-2 and the late endosomal/ lysosomal system (Jacobs *et al.*, 2013, Song *et al.*, 2017).

The identification of protein targets is much like that found in western blotting, using a sequence of primary antibodies bound to the antigen of interest and the addition of a secondary antibody with a fluorophore molecule conjugated for identification. There is also an ever-growing catalogue of commercially available antibodies, reactive with a number of species. However, instead of being performed on extracted protein from a homogenate, the analysis is performed on thin cross-sections of tissue, either frozen and cut using a cryostat or fixed and then prepared by the replacement of water with paraffin-wax so that they can be sectioned at room temperature using a microtome. These cross-sections of tissue are normally collected onto glass slides (immunohistochemistry) and stained prior to being imaged using fluorescent microscopy, but this process can also be completed with well-plates containing cells.

Current issues in immunohistochemistry relate to the accuracy and consistency of antibodies concentrations used as well as the potential for non-specific binding to proteins not of interest.

This is especially an issue when completing analysis of immunofluorescent images based on the intensity of a signal, all of which can be affected by photobleaching of conjugated fluorophore molecules and the use of the same settings during image acquisition and software analysis. Other studies relying on the counting of certain molecules and their locality to other molecules of interest are also prone to human error, an example of which is discussed comprehensively in regard to the counting of myonuclei in chapter 5 of this thesis.

Flow Cytometry

In cell and molecular biology, flow cytometry is a popular, objective method of analysing heterogenous mixtures of cells in solution to quickly profile them based on light scattering and fluorescent emissions of their intracellular and extracellular components (Adan *et al.*, 2017). An example of this can be observed in chapter 4, table 6.

This biotechnological tool is used most commonly in blood immunophenotyping for cancers and immune-suppressing diseases (over/under expression of cluster of differentiation (CD) markers but can also be used to analyse the cell cycle, detect cytokines and extra/intra-cellular protein expression.

Briefly, a flow cytometer is made up of a fluidics system which is responsible for channelling liquid containing cells/particles to a focused light source. This fluidics system comprises of two streams that meet in a central pressurised flow chamber, 1. the sheath fluid stream (usually PBS) which acts as a diluent and 2. a sample stream which is injected into the flow chamber by a pressurised airline. The joining of these two streams within the central flow chamber produces a coaxial flow based on the pressure differences between the injected sheath fluid stream and sample stream. To ensure light scattering and fluorescent emissions are representative of one cell, the sample stream pressure is always greater than the sheath fluid stream pressure creating a single cell alignment through the optical system known as hydrodynamic focusing. The rate at which cells are injected into the stream can be manipulated depending on the nature of the experiment. For example, immunophenotyping of blood cell types can be completed at a high flow rate, whereas analysis of DNA content and lowly expressed proteins would be better completed at a slow flow rate for higher resolution and accuracy. The optical system is used to channel excited light from a laser to the cell/particle and the subsequent light scatter or fluorescent light of the particle is measured with a collection optic made up of optical mirrors and filters to separate and direct specific wavelengths to their appropriate detectors. The light signals received through these filters are then converted into voltages by photodetectors and are amplified into voltage pulses which are converted from an analogue signal into digital data (Adan *et al.*, 2017).

Light scattering is produced by photons of light hitting the particle/cell and the resultant recorded light scattering produced is directly related to the structure and morphology of the cell, which can be further broken down into forward scatter (FSC) and side scatter (SSC).

FSC light is representative of the diffraction of light collected at the same angle at which the light path was formed, therefore is indicative of cell-surface area/size. SSC is a measure of the amount of reflected and refracted light that hits the cell and is therefore used as an indicator of the cells granularity and internal complexity. Additionally, collected fluorescence emissions can be quantified to give a measure of the amount of fluorescent probe bound to an intracellular or extracellular protein, and therefore the abundance of that protein available for binding of the primary antibody (Adan *et al.*, 2017).

The terms flow cytometry and FACS (fluorescence activated cell sorting) are often used interchangeably, but, the latter is a further process. Whilst flow cytometry alone can be used to identify specific characteristics of a cell whether it be size, granularity, intra/extra-cellular signalling proteins, cytokines, or miRNAs (non-coding RNA's that regulate post-transcriptional regulation of gene expression). FACS takes the principles of flow cytometry and based on light scatter and fluorescence parameters set by the researcher, a heterogenous population of cells can then be individually sorted into two or more containers; often used to produce pure populations of primary cells for culturing (e.g. removal of fibroblasts from a primary myoblast culture isolated from a muscle biopsy). Similarly, MACS (Magnetic activated cell sorting) can be used to sort heterogenous populations of cells into different cell types using a primary antibody against a unique cell-surface antigen which is then conjugated to a magnetic nanoparticle, thus allowing a specific cell type to become attached to a column with a strong magnetic field. Cells can either be separated using a) positive selection-using nano-particles conjugated with antibodies to the antigen of interest whilst cells not expressing a specific-cell surface marker pass through or b) negative selection whereby nano-particles are selected for against a cell surface marker that is not of interest; therefore, allowing the cells of interest to pass straight through a column without being magnetically attracted (Adams *et al.*, 2008). Ultimately, both methods of FACS and MACS allow for separation and purification of heterogenous populations of cells into a purified population of interest, which has greatly benefited advancements in disease and cancer diagnostics/treatment.

Whilst these techniques have traditionally been used for individual cells and small molecules, there is potential to adapt these processes for use with tissue derived in-vivo (Jackaman *et al.*, 2007), which will be explored in chapters 3 and 4. In brief, we propose that whole skeletal muscle fibers can be dispersed to produce a single muscle fibre fragment suspension suitable for flow cytometry applications. Whole skeletal muscle and muscle biopsies could then be dispersed and up to 14 fluorophores/molecular probes analysed simultaneously (Wilkerson, 2012) through simple gating processes of fluorophores. This tool holds promise for developing

a better understanding of the signalling processes in relation to hypertrophy/atrophy and multiple diseases in a time-efficient, quantitative manner in comparison to western blotting and immunohistochemistry. Using FACS systems we could also separate whole muscle fibers dependent on their myosin isoform composition to complete further biochemical analysis which would be specific to that fibre type.

Chapter 3: Study 1: Optimisation of whole murine skeletal muscle fiber dispersion for use in flow cytometry.

Introduction:

As highlighted in previous chapters, human skeletal muscle is highly complex, comprising of three myosin heavy chain (MHC) isoforms; MHC-I, MHC-IIa and MHC-IIx all of which have different capacities of maximal shortening velocity, force production per cross-sectional area of an individual muscle fiber, as well as differing resistance to fatigue. In rodents there are four MHC's expressed, MHC-I, MHC-IIa, MHC-IIc, and MHC-IIb. There are also the phenomena of hybrid fibers which contain at least two myosin isoforms and can be seen during maturation and regeneration. For example, in rodents the tibialis anterior (TA), extensor digitorum longus (EDL) serve to dorsiflex the ankle so therefore contains predominantly fast twitch muscle fibers, whereas the soleus (Sol) has a primary role to maintain stance and in slow walking so therefore contains predominately slow twitch muscle fibers capable of lower force production but with higher resistance to fatigue (Kandarian *et al.*, 1992).

Currently, proteomics research in the field of skeletal muscle growth and adaptation is performed on samples of muscle that are homogenised therefore combining a mixture of MHC isoforms and other cell types (including fibroblasts, satellite cells, nervous and connective tissues). The phosphorylation of proteins and expression of genes is then presumed to be representative of the whole muscle, despite the homogenate containing multiple non-muscle cell types and multiple muscle fiber isoforms. Whilst multiple analyses can be performed on these homogenised samples and this can give good indication of the mechanisms responding to certain stimulus within the muscle, we believe further consideration should be made to assess isoform specific changes due to their varying ability to hypertrophy and susceptibility to atrophy, each of which should be investigated independently of each other. This is especially important considering recent work that has displayed large variance in the rate of atrophy dependant on the muscle and on the muscle fiber type with satellite cells and cross-sectional area being lost at a faster rate in MHC-II isoforms and predominately fast twitch muscles (Kramer *et al.*, 2017). Other recent research has illustrated that different myosin heavy chain isoforms release different micro RNA's when damaged following crush injury

suggesting that adaptation and remodelling follows different processes in the two (Siracusa *et al.*, 2018). Investigating adaptations and responses to exercise, nutrition and pharmaceuticals could clearly therefore have a specific effect on one myosin isoform, but may have minimal effects on another myosin isoform, due to altered signalling pathways present in the remodelling and should be considered when designing an intervention.

Whilst staining of multiple antigens of interest (up to 22 channels) via flow cytometry is common practice in assessing single cell populations, this highly accurate technique has only briefly been explored to assess whole tissues rather than single cells and bodily fluids. Jackaman *et al.*, (2007) reported a method whereby individual proteins (skeletal muscle/cardiac actin, tropomyosin, dystrophin and myosin isoforms) could be detected from fresh, whole skeletal muscle and cardiac tissues in mice via flow cytometry. Briefly, fresh skeletal muscle and cardiac tissue were added to a collagenase/dispase mixture and gently triturated in order to separate the whole muscle tissue into a solution of pieces from single fibres, which was later fixed and immunofluorescently stained before being run through a flow cytometer. This method is suggested to be less labour-intensive than western blotting and immunohistochemistry and due to the protein targets, is highly applicable to diagnosing pathologies and assessing potential therapies not only in muscle, but in a variety of soft tissues. This technique also has massive potential for analysis of tissue taken in-vivo with laboratories now using flow cytometry to accurately measure up to 16 biomarkers from one single sample using a sophisticated combination of fluorescent tags, microsphere beads and fluorescent gating systems (Vignali, 2000).

Therefore, we aim to replicate this method using frozen tissue to produce a novel, quantitative method whereby we can assess myosin heavy chain isoforms and potentially muscle fiber morphology based on FSC and SSC in three different skeletal muscles. The hypothesis to be challenged was that we would observe 1. Destruction of connective tissue via collagenase treatment, therefore dispersing skeletal muscle cross-sections into a single fiber solution, 2. A higher MHC fast fluorescent intensity for fibre fragment preparations from TA and EDL than the soleus, 3. A higher MHC slow fluorescent intensity for the soleus in comparison to the TA and EDL muscles.

Methods (Single Cell Solution Optimisation of Murine Skeletal Muscle for use in Flow Cytometry):

Muscle preparation

30µm thick muscle cross-sections were cut using an OTF5000 Cryostat (Bright Instruments, UK) from the TA belonging to a Wistar Rat control limb, belonging to a previous study (Schmoll *et al.*, 2017) using an OTF5000 Cryostat (Bright Instruments, UK). Muscle cross-sections were collected into frozen 12 well plates (3-5 per well) and stored in a -80°C freezer before use in

optimisation of fiber dispersion with collagenase and for study 2 of this chapter. The section thickness was chosen so that fibre pieces would be similar in length and diameter, assuming transverse sectioning.

Collagenase I treatment

To identify an optimal protocol to create a single cell suspension from the frozen cross sections, they were each treated with different concentrations of Collagenase I/HBSS (mg/ml) (Thermo Fisher Scientific Inc, Waltham, USA) 1ml of 1mg/ml, 0.5mg/ml, 0.25mg/ml, 0.125mg/ml, 0.0625mg/ml and 0.03125mg/ml for an hour, being imaged at 5, 10, 20, 30, 45, 60 minutes with gentle trituration with a 100µl pipette based on methods adapted from Jackaman *et al.*, (2007) to aid in dispersion of single fiber units. This was completed at 24 °C within a controlled live imaging environment (Leica DMB 6000; equipped with PeCon incubation).

Imaging and analysis

Prior to being imaged DAPI (Vectashield® Antifade Mounting Medium with DAPI (1.5µg/ml), Burlingame, CA, USA) was added to the solution to identify whether collagenase was disrupting myonuclei within the single cell fragment or causing destruction of nuclei. Microscopic images were obtained at a x10 magnification from three random points within each well using the controlled live imaging environment (Leica DMB 6000; equipped with PeCon incubation). For each image, % single cell dispersion was determined by the total number of myofibers present as a single unit and not attached to any other fibers to the total number of myofibers using Image J (IBIDI, Munich, Germany).

Statistics:

Statistical software (IBM SPSS Statistics 23; Armonk, NY: IBM Corp) was used to perform all statistical analyses. To assess reproducibility of our method to disperse fibers and batch-to-batch effectiveness of the Collagenase I enzyme, we produced co-efficient of variation (COV) values also known as relative standard deviation (RSD), by dividing the standard deviation of mean % of single fiber units vs. attached fibers, by the mean % of single fiber units vs. attached fibers for each enzyme concentration and measurement time point. A lower COV/RSD value would indicate better repeatability of the single fiber dispersion.

$$Co - efficient\ of\ Variation = \frac{Standard\ Deviation}{Mean}$$

Two way within-subjects ANOVA's were also completed where enzyme concentration, time of incubation with Collagenase I enzyme and the interaction effects were explored.

Results:

There was a significant main effect for enzyme concentration ($F_{6,12}= 833.16$, $P=0.0001$) as well as a significant main effect for time ($F_{6,12}= 593.67$, $P=0.0001$) on percentage single fiber dispersion. There was a significant interaction effect for time and enzyme concentration ($F_{36,72}= 42.97$, $P=0.0001$) on percentage single fiber dispersion.

There was a significantly greater mean percentage single fiber dispersion using a 1mg/ml (91.89 ± 4.05) concentration in comparison to 0.0625mg/ml (65.29 ± 4.2), 0.03125 (36.11 ± 6.66), and the HBSS control (14.13 ± 1.16) after 60 minutes, ($P<0.05$). There were no significant differences between mean percentage single fiber dispersion at 60 minutes between 1mg/ml, 0.5mg/ml (88.99 ± 3.04), 0.25mg/ml (83.89 ± 3.52) and 0.125 mg/ml (88.02 ± 3.55), ($P > 0.05$). However, after 45 minutes of treatment with 1mg/ml and 0.5mg/ml concentrations, and 60 minutes with a 0.125mg/ml concentration fibers began to fragment and nuclei destroyed (Figure 2D), therefore making them unsuitable for staining. Therefore, fiber pieces were optimally dispersed (highest percentage of single fiber units vs attached fibres-without degradation/fragmentation), after 60 minutes without any sign of degradation, using 0.125mg/ml concentration of Collagenase I at 24 °C.

The mean COV value for all Collagenase I enzyme concentrations, used across all time points measured was 7.2%, and the mean COV value for 0.125mg/ml Collagenase I was 5.47%, illustrating the reproducibility of the treatment on muscle cross-sections. Whilst data presented here illustrates single fiber dispersion using TA cross-sections, preliminary experiments displayed that EDL and soleus skeletal muscle cross-sections were effectively dispersed into single fibers despite differences in connective tissue between the different muscles (results not shown).

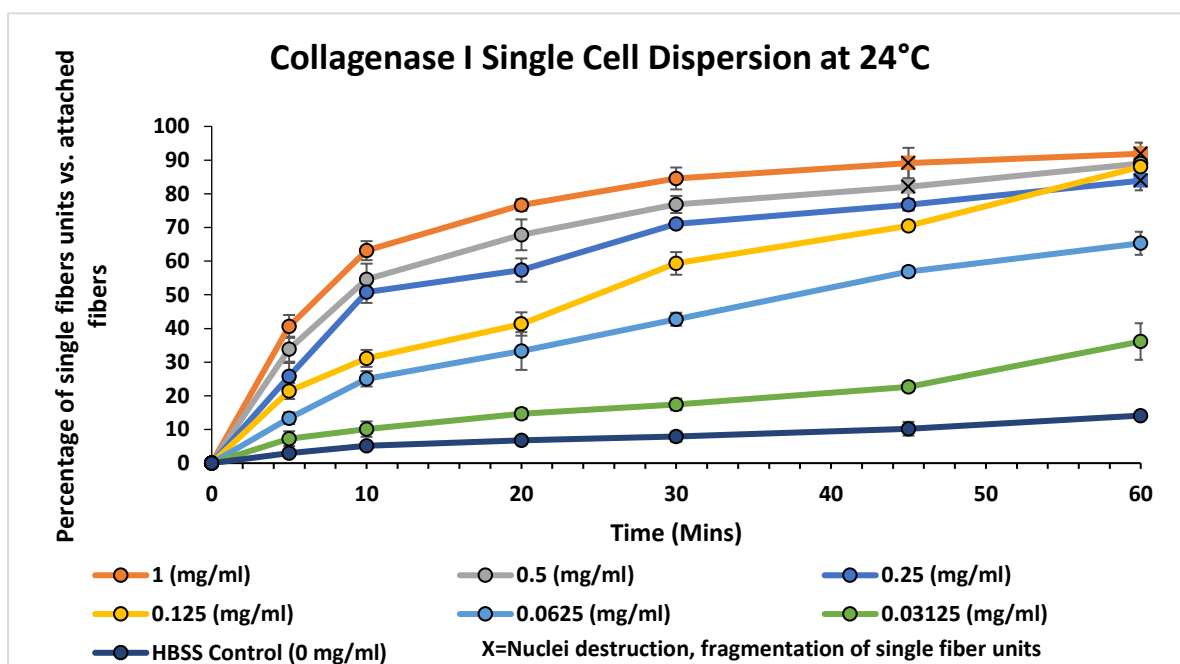


Figure 1: Effectiveness of Collagenase I concentrations on single muscle fiber dispersion of TA skeletal muscle at 24°C. Mean \pm SD.

Table 1: Co-efficient of Variation (%) for the % total number of myofibers present as a single unit and not attached to any other fibers to the total number of attached myofibers.							
Time	1 (mg/ml)	0.5 (mg/ml)	0.25 (mg/ml)	0.125 (mg/ml)	0.0625 (mg/ml)	0.03125 (mg/ml)	HBSS Control
0	0.0	0.0	0.0	0.0	0.0	0.0	0.0
5	8.4	11.0	15.2	11.0	13.0	30.4	0.0
10	4.5	8.6	6.3	8.1	9.1	22.6	13.6
20	2.2	6.8	6.0	8.4	16.8	10.2	4.9
30	3.9	3.3	1.3	5.7	4.5	9.7	19.2
45	5.1	8.6	2.1	1.8	2.5	5.5	20.1
60	3.6	2.8	3.4	3.3	5.3	15.1	6.7
Mean Co-Efficient of Variation: 7.2 \pm 6.6%							

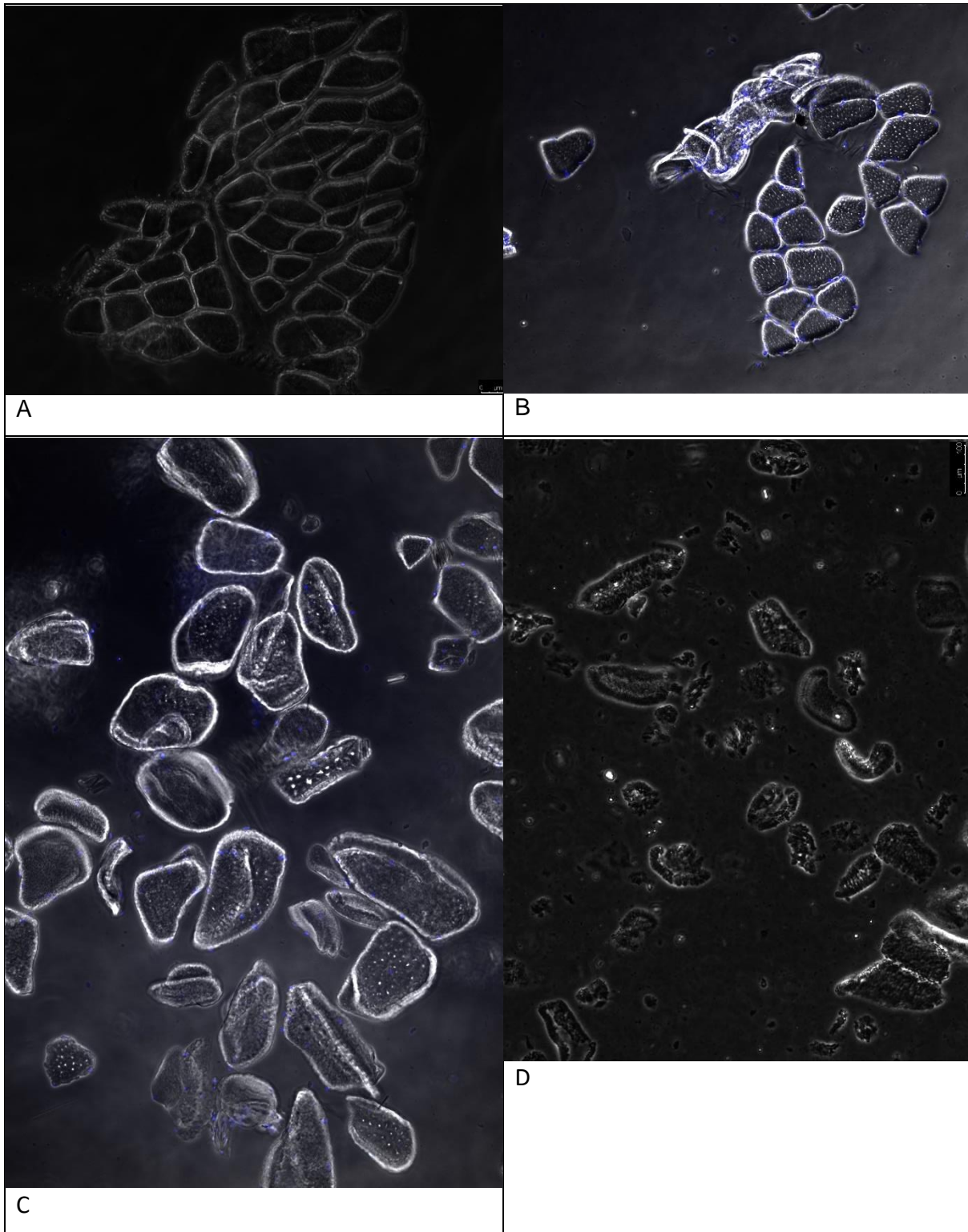


Figure 2: A= Phase contrast of image Cross section at 0 minutes of 0.125mg/ml Collagenase I treatment at 22°C. B= Phase contrast/DAPI overlay of cross section dispersion after 15 minutes of 0.125mg/ml Collagenase I treatment at 22°C. C= Phase contrast/DAPI overlay of single fiber fragments after 30 minutes of 0.125mg/ml Collagenase I treatment at 22°C. D= Phase contrast image of destruction of single fiber units after 30 minutes of 1mg/ml Collagenase I treatment at 24°C.

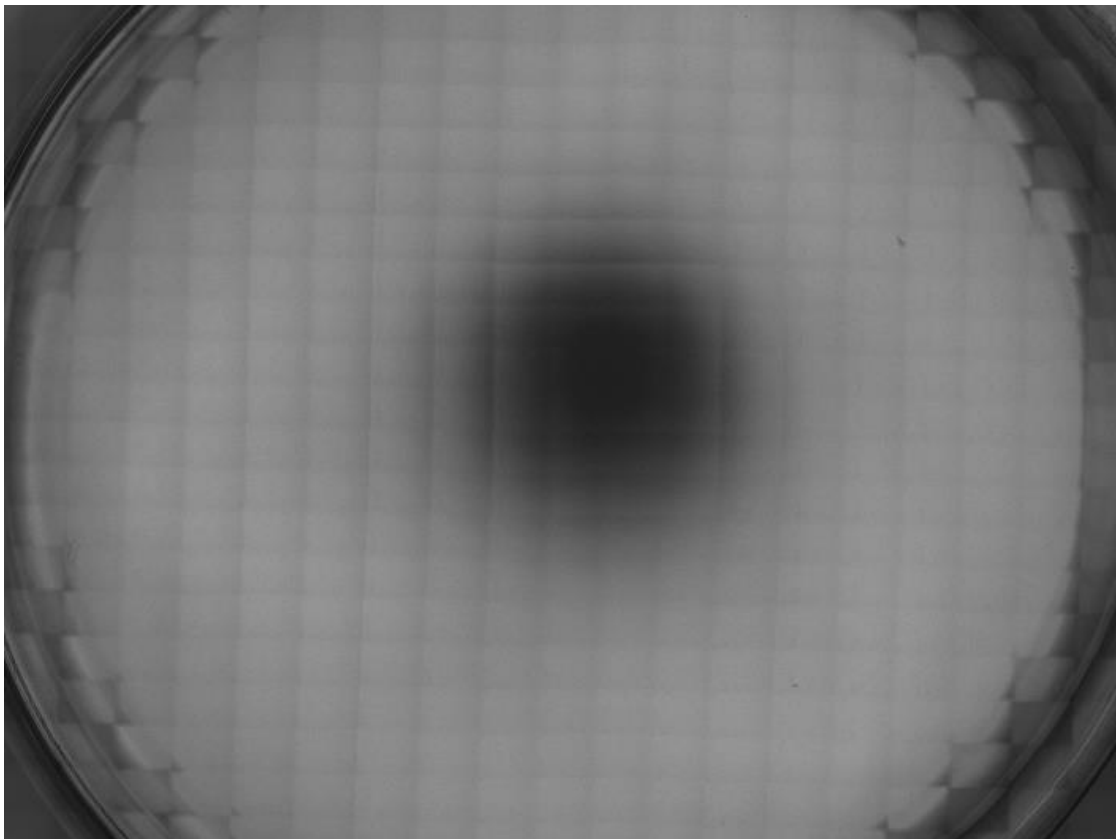
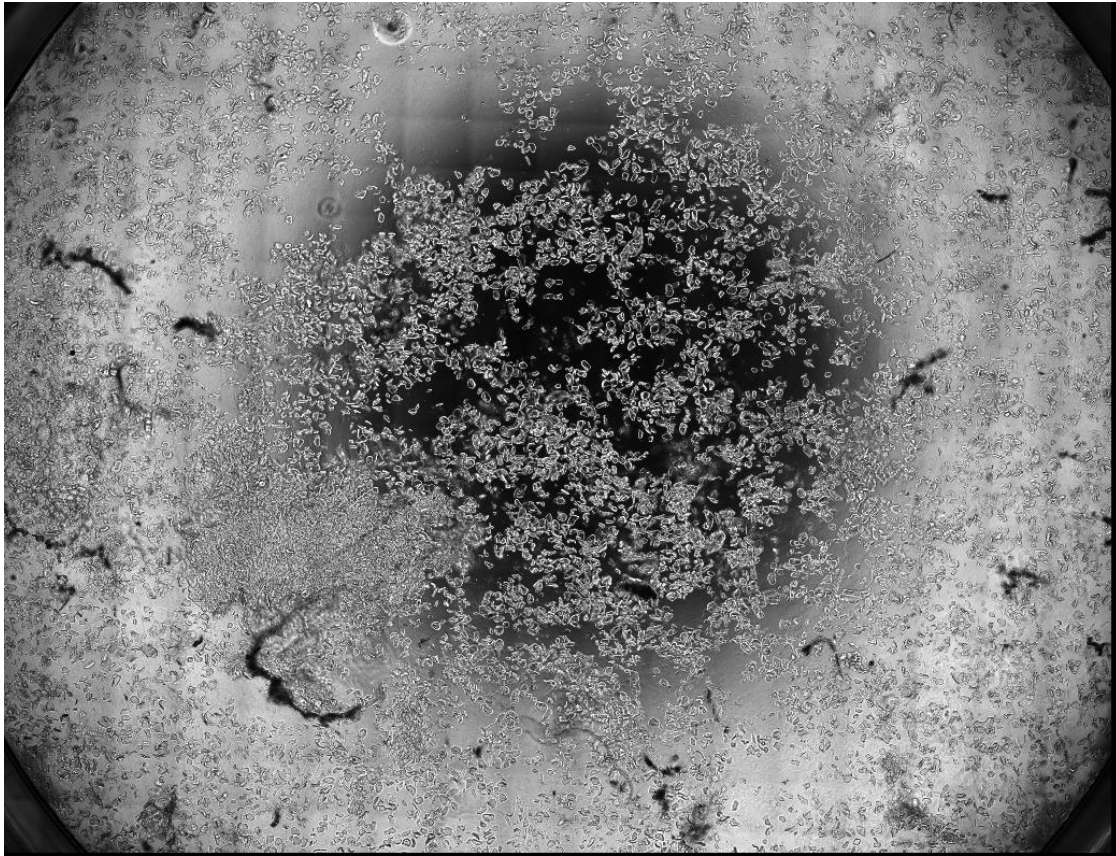


Figure 3: Example of optimally dispersed single muscle fiber units after 30 minutes of 0.125mg/ml at 24°C of Collagenase I vs empty well containing Collagenase I.

Conclusion:

We have demonstrated that whole skeletal muscle cross-sections can be dispersed into a single fiber solutions without degradation of fibers using 0.125mg/ml of Collagenase I between after 60 minutes at 24°C. This method is reproducible, indicated by the COV mean of 7.6% between lot-to-lot experiments for differing concentrations of Collagenase I across all time-points measured.

Chapter 3: Study 2: Assessment of fiber size and type via flow cytometry using whole murine skeletal muscles.

Methods:

Single fiber dispersion

As outlined in study 1, 30µm TA, EDL and soleus muscle cross-sections from a control Wistar rat (Schmoll *et al.*, 2017) were cut (in series) and placed into a frozen 12-well plate (3-5 per well) and treated with 0.125mg/ml Collagenase I for 45-60 minutes at 24°C. 1ml of 2% paraformaldehyde was added per well to fix the fiber pieces for 1 hour in the dark before solutions were transferred to an Eppendorf.

Muscle Fiber Typing

Single Cell Solution

A method used to prepare cultured C2C12 cells for flow cytometry was modified for the fibre fragment solutions. Single fiber solutions were spun at 1200rpm for 5 minutes and paraformaldehyde removed.

Fragments were washed for 5 minutes x3 in HBSS before being incubated for 20 minutes in horse serum. Serum was washed off for 5 minutes in HBSS and primary antibodies for MYHC Slow (1in10 PBS), MYHC Fast (1in100 PBS) for 1 hour. The primary antibodies were washed off for 5 minutes x3 in HBSS and secondary antibody added (Biotinylated Horse Anti-Mouse IgG Antibody, rat adsorbed, Vector Laboratories Inc., Burlingame, CA, USA) for 30 minutes. The secondary antibody was washed off for 5 minutes x3 in HBSS before the fluorescent tag (Fluorescein Avidin D, Vector Laboratories Inc., Burlingame, CA, USA) was added in the dark and incubated for 30 minutes. A further wash was performed for 5 minutes x2 in HBSS before fiber fragments were broken from the pellet back into solution for use in the flow cytometer. Single fiber solutions were stained individually for each MHC isoform.

Untreated controls were also used for each individual sample as all cells emit some levels of natural fluorescence (autofluorescence) from molecules such as NADH, collagen and aromatic amino acids (350-550nm). Positive controls were produced using Vybrant™ DiO

Cell-Labeling Solution (Thermo Fisher Scientific Inc, Waltham, USA) which will stain all protein. C2C12 myoblast cells were also used with DiO labelling solution as a further control.

Histology and imaging

To confirm any results of our flow cytometry, we performed immunohistochemistry on 10µm cross-sections that were cut from the TA, EDL and soleus muscles and collected onto Thermo Scientific™ SuperFrost Plus™ Adhesion slides (Thermo Fisher Scientific Inc, Waltham, USA) and fixed in acetone for 10 minutes. A ring was drawn around cross-sections using a PAP pen. Sections were then washed for 5 minutes x3 in PBS. Sections were incubated for 20 minutes in horse serum (the serum in which the secondary antibody was produced to block any non-specific binding). Serum was washed off for 5 minutes in PBS and primary antibodies for MYHC Slow (1in10 PBS), MYHC Fast (1in100 PBS) for 1 hour. The primary antibodies were washed off x2 for 5 minutes in PBS and secondary antibody added (Biotinylated Horse Anti-Mouse IgG Antibody, rat adsorbed, Vector Laboratories Inc., Burlingame, CA, USA) for 30 minutes. The secondary antibody was washed off for 5 minutes x3 in PBS before the fluorescent tag (Fluorescein Avidin D, Vector Laboratories Inc., Burlingame, CA, USA) was added in the dark and incubated for 30 minutes. A further wash was performed for 5 minutes x2 before coverslips were fixed with mounting medium containing DAPI (Vectashield® Antifade Mounting Medium with DAPI (1.5µg/ml), Burlingame, CA, USA). Tlescan images of the entire cross-sections were performed for the MHC isoform and DAPI using a (Leica DMB 6000, Wetzlar, Germany) and fluorescent channels overlaid.

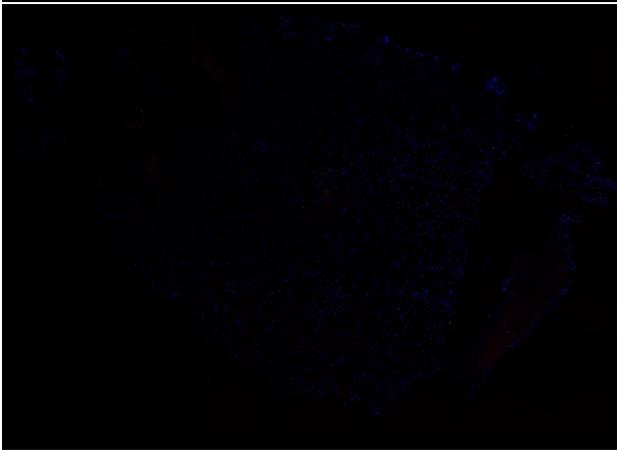
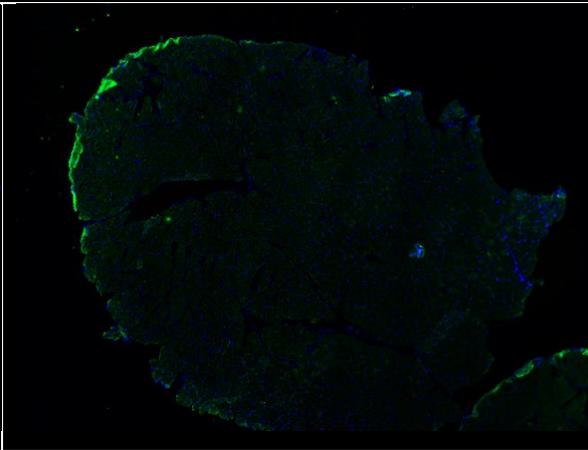
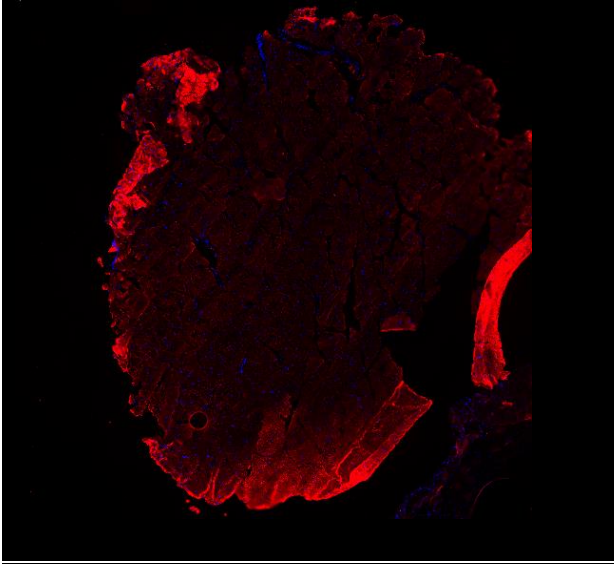
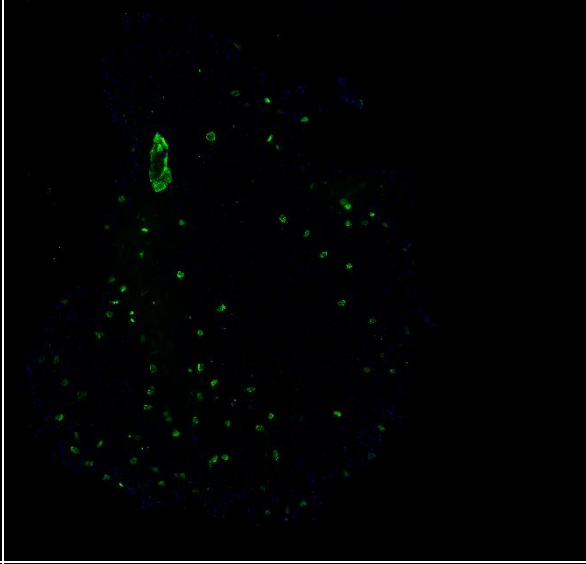
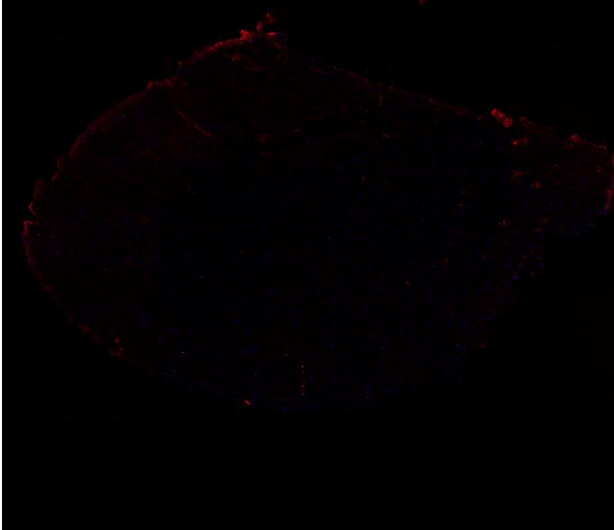
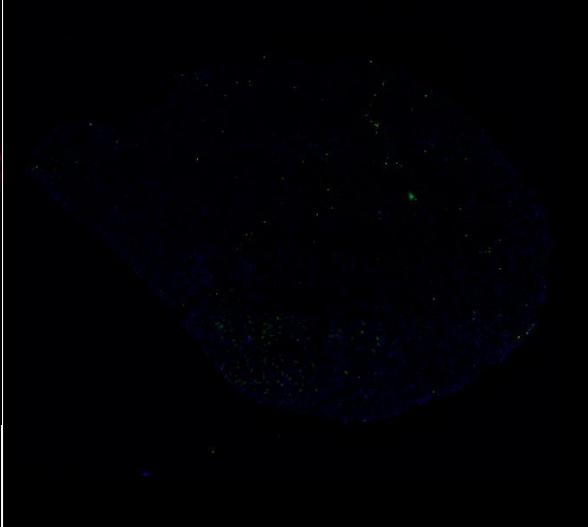
Flow Cytometry:

The samples were analysed using flow cytometry on a BD Accuri C6 flow cytometer with BD CFlow® Software, collecting 2000 events per sample on a medium flow rate. Gating was applied, labelled as P1 to remove any small debris from analysis (endothelial/nervous/connective tissue) SSC-A, FSC-A and FL1 values were exported to characterize fluorescein fluorescent intensity.

Statistics:

All statistical analyses of FSC-A, SSC-A and fluorescent intensity (FI) were performed using one-way between group ANOVA's on SPSS (v.24.0; SPSS, Chicago, IL, USA). Mean comparisons were assessed for FSC-A and SSC-A between skeletal muscle types, untreated skeletal muscle controls and C2C12 cells. Mean comparisons were also made for FL1-A between both muscle type and MHC isoform. Results are presented as Mean ± SE.

Table 2: Identification fiber type percentage using immunohistochemistry. *Our percentage of fast and slow myosin heavy chain isoforms were in line with previous findings. (Soukup et al., 2002; Tasić et al., 2011).*

	
<p>Soleus Fast = 2%</p>	<p>Soleus Slow = 98%</p>
	
<p>EDL Fast = 91.6%</p>	<p>EDL Slow = 8.4%</p>
	
<p>TA Fast = 96.17%</p>	<p>TA Slow = 3.83%</p>

Results:

FSC-A Group Differences

The mean FSC-A for TA ($7,616,143 \pm 1,423,839$) was not significantly different ($P=0.982$) in comparison to the mean EDL FSC-A ($7,499,083 \pm 1,559,612$), the mean soleus FSC-A ($7,839,470 \pm 2,381,724$, $P<0.966$) and the mean C2C12 FSC-A ($7,361,343 \pm 2,565,489$, $P<0.176$). The mean EDL FSC-A was also not significantly different than the soleus ($P=0.948$) and C2C12 ($P=0.169$) FSC-A. There was no significant difference between Soleus FSC-A and the C2C12 FSC-A ($P=0.189$), (Tables 3-5, Column 1).

SSC-A Group Differences

The mean SSC-A for TA ($3,665,319 \pm 123,521$) was not significantly higher ($P=0.184$) than mean EDL SSC-A ($3,564,136 \pm 215,103$) but was significantly higher ($P<0.0001$) than the mean soleus SSC-A ($3,393,722 \pm 412,990$) and the mean C2C12 SSC-A ($1,674,980 \pm 629,488$). The mean EDL FSC-A was also significantly higher than the soleus ($P<0.03$) and C2C12 ($P<0.0001$) FSC-A. Soleus FSC-A was also significantly higher than the C2C12 FSC-A ($P<0.0001$). This shows the similarity in size between TA and EDL (predominately fast twitch) fiber pieces, whilst the soleus fiber piece SSC-A were significantly lower, as expected as soleus is a predominately slow twitch muscle containing smaller fibers. The significant difference between all skeletal muscle fiber pieces and the C2C12 myoblast cells was also expected due to the size difference between an individual myoblast and a myofiber diameter, (Tables 3-5, Column 3).

MHC Fluorescent Intensity

There were no significant differences between the mean control TA fluorescent intensity ($29,362 \pm 5247$), the mean control EDL fluorescent intensity ($27,479 \pm 6585$, $P=0.998$), the mean control Soleus fluorescent intensity ($59,686 \pm 36366$, $P=0.970$) and the mean control C2C12 fluorescent intensity (8649 ± 265 , $P=0.970$). The lower C2C12 fluorescent intensity although not significantly different, is presumed to be from the reduced complexity of the cell in comparison to myofibers, therefore emitting less auto-fluorescence.

TA Fast MHC isoform fluorescent intensity ($1,879,072 \pm 158,876$) was not significantly different than the EDL Fast MHC isoform fluorescent intensity ($1,771,734 \pm 245,495$, $P=0.893$) or the Soleus Fast MHC isoform fluorescent intensity ($3,036,381 \pm 570,718$, $P=0.154$). These results were unexpected due to the lack of fast MHC isoform present in the soleus muscle.

TA Fast MHC isoform fluorescent intensity was not significantly different in comparison to the TA Slow MHC isoform fluorescent intensity ($1,821,531 \pm 300,215$, $P=0.943$). There was no significant difference between the EDL Fast MHC isoform fluorescent intensity and the Soleus

Fast MHC isoform fluorescent intensity ($P=0.12$) or higher than EDL Slow MHC isoform fluorescent intensity ($2,060,197 \pm 277,557$, $P=0.193$). Both the TA and EDL are predominately fast twitch muscles, approximately 95% Fast vs 5% Slow. Whilst this trend can be observed in these results, we would expect the difference between these isoforms to be significantly greater.

Soleus Fast MHC isoform fluorescent intensity was not significantly different in comparison to the Soleus Slow MHC isoform fluorescent intensity ($2,824,846 \pm 247,552$, $P=0.791$). When compared to our immunohistochemistry, we would expect these results to show the opposite trend with Soleus Slow MHC isoform fluorescent intensity being significantly higher than the Fast isoform as it is a predominately slow twitch muscle.

TA Slow MHC isoform fluorescent intensity was not significantly different than the EDL Slow MHC isoform fluorescent intensity ($P=0.765$) and Soleus Slow MHC isoform fluorescent intensity ($P=0.214$). EDL Slow MHC isoform fluorescent intensity was not significantly different than the Soleus Slow MHC isoform fluorescent intensity ($P=0.341$). Both predominately fast twitch muscles expressed lower (although this did not reach significance) slow MHC isoform fluorescent intensity in comparison to the Soleus as hypothesised. See Tables 3-5, Column 2.

DiO Fluorescent Intensity-Proxy Marker for protein content

The mean TA DiO fluorescent intensity ($8,061,223 \pm 1,025,116$) was not significantly different from the EDL DiO fluorescent intensity ($8,518,127 \pm 467,141$, $P=0.568$) or the Soleus DiO fluorescent intensity ($8,753,615 \pm 2,263,658$, $P=0.388$), however was significantly higher than the C2C12 DiO fluorescent intensity ($5,582,295 \pm 1,451,303$, $P=0.002$). The EDL DiO fluorescent intensity was not significantly different to the Soleus DiO fluorescent intensity ($P=0.768$), but was significantly higher than the C2C12 DiO fluorescent intensity ($P=0.0001$). The Soleus DiO fluorescent intensity was also significantly higher than the C2C12 DiO fluorescent intensity ($P=0.05$).

The mixed population of DiO stained C2C12 cells fluorescent intensity ($3,487,345 \pm 378,067$) had a significantly lower fluorescent intensity in comparison to the C2C12 DiO fluorescent intensity ($P=0.005$) and a significantly higher fluorescent intensity in comparison to the C2C12 control fluorescent intensity (8649 ± 265 , $P=0.0001$). These results illustrate the ability of flow cytometers to distinguish between populations of stained, unstained and mixed populations of fiber pieces/cells, (Table 6).

Table 3: TA Control, anti-SLOW, anti-Fast, DiO, Mean \pm SD

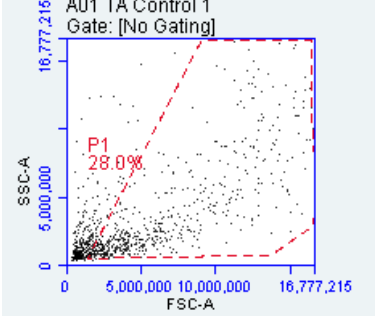
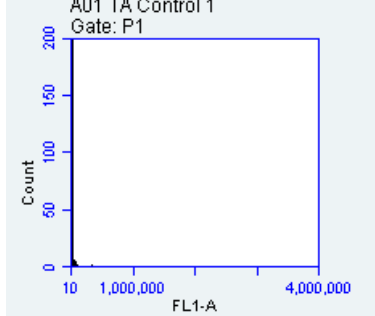
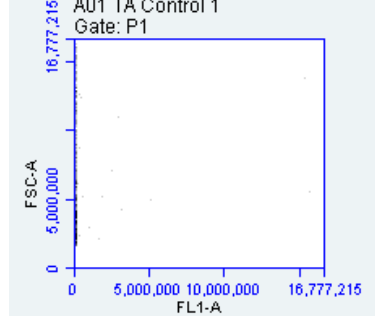
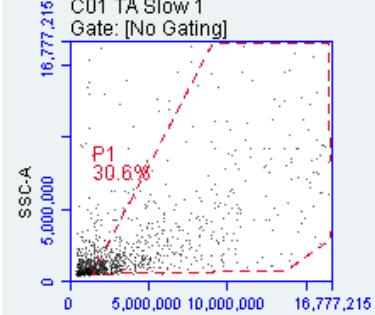
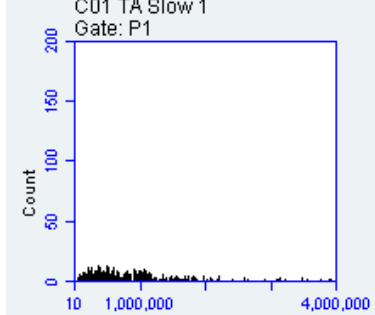
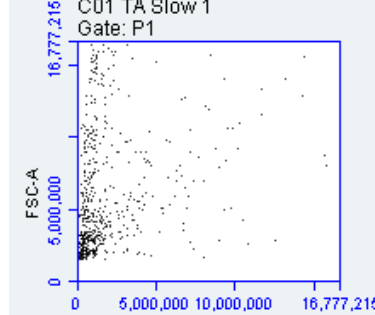
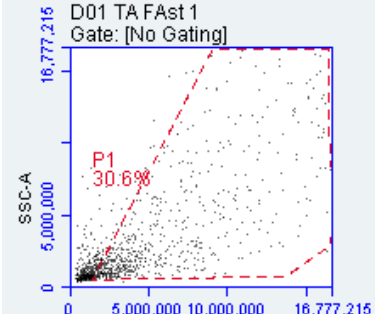
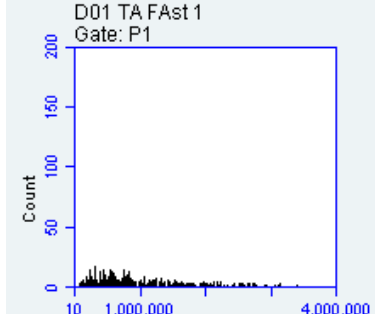
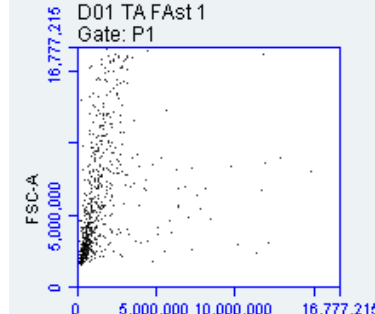
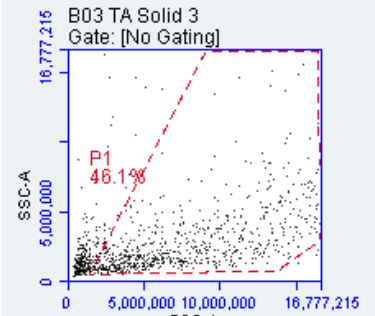
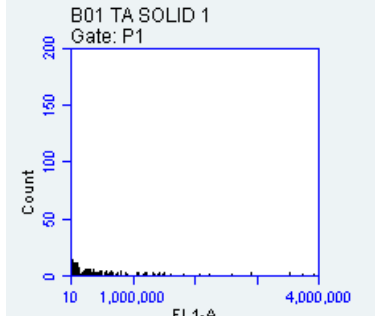
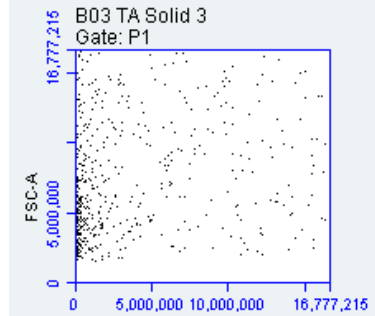
<p>A01 TA Control 1 Gate: [No Gating]</p> 	<p>A01 TA Control 1 Gate: P1</p> 	<p>A01 TA Control 1 Gate: P1</p> 
<p>SSC: 3,694,711 \pm 196,955</p>	<p>FL1-A: 29,362 \pm 5247</p>	<p>FSC: 6,813,860 \pm 260,546</p>
<p>C01 TA Slow 1 Gate: [No Gating]</p> 	<p>C01 TA Slow 1 Gate: P1</p> 	<p>C01 TA Slow 1 Gate: P1</p> 
<p>SSC: 3,361,792 \pm 186,146</p>	<p>FL1-A: 1,821,531 \pm 300,215</p>	<p>FSC: 6,616,830 \pm 482,005</p>
<p>D01 TA FAs1 Gate: [No Gating]</p> 	<p>D01 TA FAs1 Gate: P1</p> 	<p>D01 TA FAs1 Gate: P1</p> 
<p>SSC: 3,801,069 \pm 206,687</p>	<p>FL1-A: 1,879,072 \pm 158,876</p>	<p>FSC: 6,801,804 \pm 223,572</p>
<p>B03 TA Solid 3 Gate: [No Gating]</p> 	<p>B01 TA SOLID 1 Gate: P1</p> 	<p>B03 TA Solid 3 Gate: P1</p> 
<p>SSC: 3,803,705 \pm 143,425</p>	<p>FL1-A: 10,232,080 \pm 371367</p>	<p>FSC: 10,232,080 \pm 371,367</p>

Table 4: EDL Control, anti-SLOW, anti-Fast, DiO

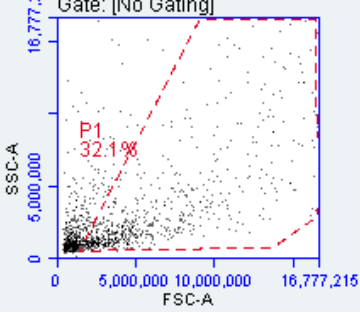
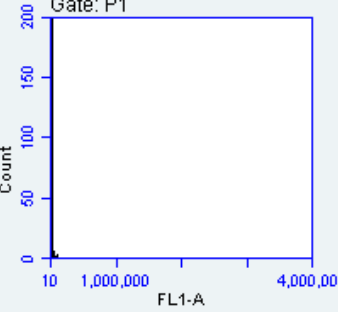
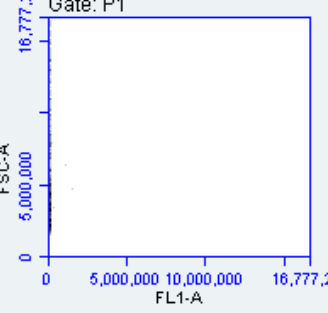
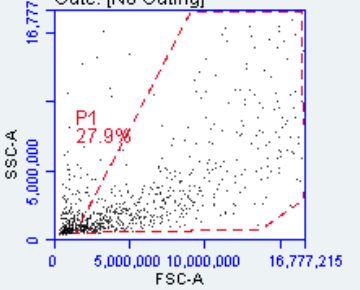
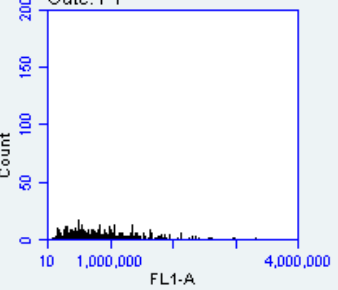
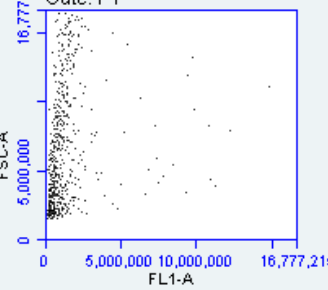
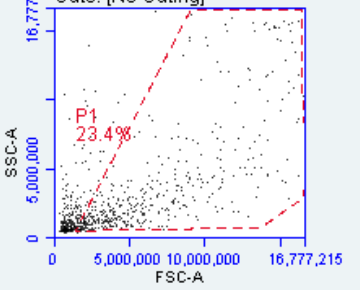
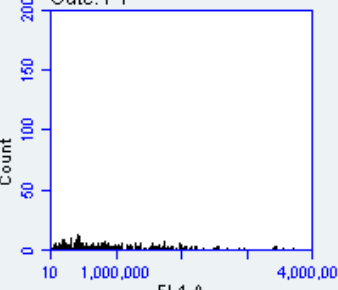
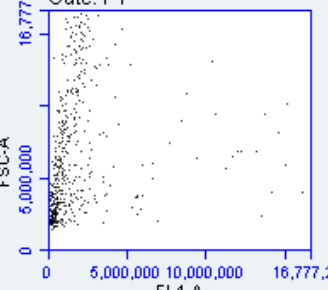
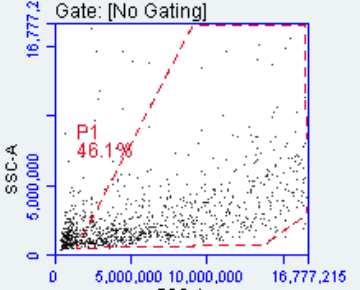
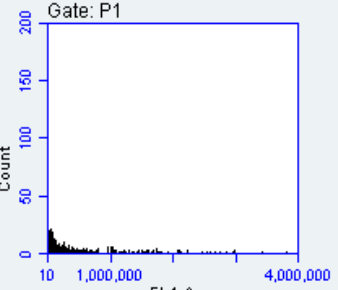
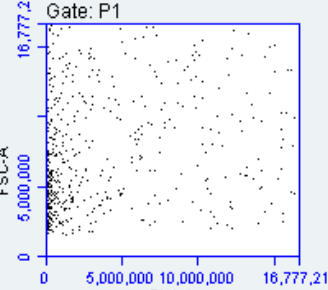
<p>A03 EDL Control 3 Gate: [No Gating]</p> 	<p>A03 EDL Control 3 Gate: P1</p> 	<p>A03 EDL Control 3 Gate: P1</p> 
<p>SSC: 3,343,601 ± 176,373</p>	<p>FL1-A: 27,479 ± 6585</p>	<p>FSC: 6,659,800 ± 458,742</p>
<p>C03 EDL Slow 3 Gate: [No Gating]</p> 	<p>C03 EDL Slow 3 Gate: P1</p> 	<p>C03 EDL Slow 3 Gate: P1</p> 
<p>SSC: 3,402,125 ± 99,888</p>	<p>FL1-A: 2,060,197 ± 277557</p>	<p>FSC: 2,060,197 ± 277,557</p>
<p>D03 EDL Fast 3 Gate: [No Gating]</p> 	<p>D03 EDL Fast 3 Gate: P1</p> 	<p>D03 EDL Fast 3 Gate: P1</p> 
<p>SSC: 3,890,945 ± 205,655</p>	<p>FL1-A: 1,771,734 ± 245,494</p>	<p>FSC: 1,771,734 ± 245,494</p>
<p>B03 EDL Solid 3 Gate: [No Gating]</p> 	<p>B03 EDL Solid 3 Gate: P1</p> 	<p>B03 EDL Solid 3 Gate: P1</p> 
<p>SSC: 3,619,872 ± 205,815</p>	<p>FL1-A: 8,518,127 ± 467,141</p>	<p>FSC: 9,985,746 ± 319,304</p>

Table 5: Soleus Control, anti-SLOW, anti-Fast, DiO

<p>E01 Sol Control 1 Gate: [No Gating]</p> <p>P1 21.3%</p>	<p>E01 Sol Control 1 Gate: P1</p> <p>Count</p> <p>FL1-A</p>	<p>E01 Sol Control 1 Gate: P1</p> <p>FSC-A</p> <p>FL1-A</p>
<p>SSC: 3,310,171 ± 117,333</p>	<p>FL1-A: 59,686 ± 36,366</p>	<p>FSC: 6,620,575 ± 307,811</p>
<p>G01 Sol SLOW 1 Gate: [No Gating]</p> <p>P1 22.5%</p>	<p>G01 Sol SLOW 1 Gate: P1</p> <p>Count</p> <p>FL1-A</p>	<p>G01 Sol SLOW 1 Gate: P1</p> <p>FSC-A</p> <p>FL1-A</p>
<p>SSC: 2,863,030 ± 49,257</p>	<p>FL1-A: 2,824,846 ± 247,552</p>	<p>FSC: 5,8383,06 ± 175,794</p>
<p>H01 Sol Fast 1 Gate: [No Gating]</p> <p>P1 27.6%</p>	<p>H01 Sol Fast 1 Gate: P1</p> <p>Count</p> <p>FL1-A</p>	<p>H01 Sol Fast 1 Gate: P1</p> <p>FSC-A</p> <p>FL1-A</p>
<p>SSC: 3,524,176 ± 218,476</p>	<p>FL1-A: 3,036,381 ± 570,718</p>	<p>FSC: 3,036,381 ± 570,718</p>
<p>F01 Sol SOLID Gate: [No Gating]</p> <p>P1 46.4%</p>	<p>F01 Sol SOLID Gate: P1</p> <p>Count</p> <p>FL1-A</p>	<p>F01 Sol SOLID Gate: P1</p> <p>FSC-A</p> <p>FL1-A</p>
<p>SSC: 3,877,512 ± 125,433</p>	<p>FL1-A: 8,753,615 ± 2,263 658</p>	<p>FSC: 11,635,658 ± 4,287,997</p>

Table 6: C2C12 Control vs 100% Stained FITC vs 50% Stained FITC

<p>F09 C2C12 Control 1 Gate: [No Gating] P1 95.2%</p>	<p>F09 C2C12 Control 1 Gate: P1</p>	<p>F09 C2C12 Control 1 Gate: P1</p>
<p>SSC: 1,643,572 ± 71,614</p>	<p>FL1-A: 8649 ± 265</p>	<p>FSC: 8,655,894 ± 179,258</p>
<p>G09 C2C12 Stained 1 Gate: [No Gating] P1 92.9%</p>	<p>G09 C2C12 Stained 1 Gate: P1</p>	<p>G09 C2C12 Stained 1 Gate: P1</p>
<p>SSC: 2,123,509 ± 76,323</p>	<p>FL1-A: 5,582,295 ± 1,451,303</p>	<p>FSC: 8,339,611 ± 463,248</p>
<p>H11 C2C12 Mixed 3 Gate: [No Gating] P1 92.4%</p>	<p>H11 C2C12 Mixed 3 Gate: P1</p>	<p>H11 C2C12 Mixed 3 Gate: P1</p>
<p>SSC: 1,825,511 ± 43,017</p>	<p>FL1-A: 378,067 ± 23,000</p>	<p>FSC: 7,523,450 ± 166,201</p>

Overall Discussion

The aim of these studies was to produce a single fiber solution of frozen skeletal muscle tissue suitable for flow cytometry application, for identification of MHC fast and slow isoforms in various skeletal muscles. The hypothesis was that we would observe 1. Destruction of connective tissue via collagenase treatment, therefore dispersing skeletal muscle cross-

sections into a single fiber solution, 2. A higher MHC fast fluorescent intensity for TA and EDL than the soleus, 3. A higher MHC slow fluorescent intensity for the soleus in comparison to the TA and EDL muscles.

In summary, we were able to successfully produce a single fiber solution from whole frozen skeletal muscle tissue from a TA, EDL and soleus. We found this protocol to be repeatable with little variation between treatments and useful on all three muscle types using 0.125mg/ml of Collagenase I at 24°C for 45 minutes, which gave the most amount of single fibers without destruction of fiber pieces. This was confirmed by phase contrast tilescan imaging of dispersed muscle cross-sections into single fiber units within a 12-well plate. We were also able to perform immunocytochemistry on these fiber pieces individually with MHC fast and slow isoforms, although our results didn't match our immunohistochemistry results.

Assessing fiber piece morphology using FSC-A/SSC-A

Jackaman *et al.*, (2007) illustrate that after dispersion of the soleus and quadricep muscles that the resultant single fiber solution produces a strict population of fiber pieces much like the FSC/SSC produced by C2C12 cells (Column 1, Table 6). However, our fiber dispersion produces a more varied population as observed in Column 1 of tables 3-5. We propose that this may be due to the structural integrity of these fiber pieces as they flow through a pressurised system before light scatter and fluorescence is measured. As the original paper utilises fresh muscle samples that has not been flash frozen and thawed, it may be that the structural integrity is maintained to a better extent when using fresh tissue. However, we are also sceptical about the original papers reporting's, as this technique has not been used since in any published work as far as we are aware despite the potential benefits. We also cannot confirm that our single fiber pieces are passing through the fluidics system without folding over or as a single unit as would happen with a normal population of single cells. This may provide some evidence as to why FSC/SSC is so varied despite confirmation that muscle cross-sections are appropriately dispersed within a well. Certain flow cytometers provide microscopic snapshots of cells as they pass through the system which may be useful in future analysis.

Despite the large variation in FSC scatter, the mean FSC (a measure of granularity) did not differ between any of the muscle types confirming that our fiber pieces were all the same thickness following the sectioning of the cross-sections (30µm).

As highlighted in the immunohistochemistry, TA and EDL are predominately fast twitch muscles and their fiber diameters are in general larger than slow twitch fiber diameters, like that found in a predominately slow twitch muscle such as the soleus (Table 2). Understanding this, we have produced evidence that this technique can be used to measure fiber diameter as mean SSC, (a measure of cell size) was significantly higher in the TA ($P < 0.0001$) and EDL

($P < 0.03$) in comparison to the soleus muscle fiber pieces. All skeletal muscle fiber pieces also had a greater mean SSC in comparison to C2C12's ($P < 0.0001$), as would be expected when comparing a muscle fiber diameter to the diameter of a C2C12 cell (Mackey & Kjaer, 2017).

Skeletal muscle MHC isoform determination via fluorescent intensity

We hypothesised that the TA and EDL would have produce higher MHC Fast mean fluorescent intensities in comparison to the soleus, and the soleus would have higher MHC Slow mean fluorescent intensities. Whilst our immunohistochemistry results staining muscle cross-sections on slides were as expected, these results did not correspond to our flow cytometry data. MHC Fast mean fluorescent intensity was higher in the soleus muscle in comparison to the TA and EDL and was approaching significance ($P = 0.15$), although we would expect limited fluorescence of MHC fast in the slow twitch soleus muscle. MHC Slow mean fluorescent intensity was also higher in the soleus in comparison to the TA ($P = 0.214$) and EDL ($P = 0.341$) as would be expected. In fact, only the EDL muscle presented MHC Fast/Slow mean fluorescent intensities in the correct ratio to the immunohistochemistry results although they were not significantly different ($P = 0.193$)

Whilst we previously report successful dispersion of muscle cross-sections into single fiber solutions, the staining of these pieces and their detection by the flow cytometer is difficult to explain. Despite all immunostained fiber solutions producing significantly higher levels of FL1-A intensity in comparison to their controls ($P < 0.001$), there is a potential of non-specific binding producing fluorescence that is not from the antigen of interest. Future investigations should look to use antibodies bound to fluorophores outside of the natural range of autofluorescence ($> 510\text{nm}$). Despite fixing and blocking with serum from which the secondary antibody was produced in, the effectiveness of this acting on the muscle fiber pieces within an Eppendorf is not well understood. Also, we propose that as soleus cross-sections were undoubtedly the smallest muscle cross-sections used then there was less material per well in comparison to the TA and EDL cross sections. Therefore, concentrations of primary antibody, secondary antibody and fluorescent tag used with the soleus would then therefore be exposed to less material producing higher binding levels and therefore FL1-A intensity. Supporting this idea, FL1-A values for Soleus were consistently higher in both MHC Fast and Slow in comparison to the TA and EDL, thus providing evidence that antibody concentrations should be more tightly controlled in future experiments.

Conclusion:

Whilst our initial results hold some promise for the use of flow cytometry to assess whole murine skeletal muscle tissue proteins, the process is not as simple and straight forward as first indicated by Jackaman *et al.*, (2007). The fragility and suitability of our fiber pieces to pass through a flow cytometer and the effectiveness of blocking and immunostaining these pieces

with the appropriate antigen of interest need to be further assessed. Future studies should consider producing more robust staining procedures of single fiber solutions isolated from frozen tissues in order to accurately assess skeletal muscle isoforms and proteins.

Chapter 4: Nuclear Density in muscular atrophy and recovery from atrophy

Introduction:

Skeletal muscle, responsible for locomotion and with a key function in the balance of stored protein and carbohydrate, is the most abundant tissue in the human body and, therefore, maintenance and adaptation of its structure and function are key throughout the animal kingdom. Preservation of muscle mass and quality during disease and ageing are currently key areas of research as the number of people aged over 65 is predicted to rise by 19% in the next decade and will contribute to a 37% increase in the number of persons living with disabilities ascribed to musculoskeletal disease (Guzman-Castillo *et al.*, 2017). As skeletal muscle cells are post-mitotic, changes in myofiber size are governed by the rate at which protein synthesis and breakdown occur, allowing for phenotypical remodelling of the abundance and expression profiles for individual muscle protein isoforms (Cobley *et al.*, 2016). Clearly, through the altered expression of gene profiles and their resultant protein products skeletal muscle is highly malleable, without the need for cellular apoptosis or regeneration (Hoppeler, 2016).

Resistance training (mechanical stimuli) and protein ingestion promote a positive protein balance, defined as a positive ratio of synthesis to degradation and subsequent hypertrophy of the muscle through the IGF-1/Akt and mTOR-PS6K signalling pathways (Areta *et al.*, 2014; Damas *et al.*, 2015). Conversely, a negative net protein balance is predictive of muscular atrophy (a reduction in myofibrillar volume), driven by the ubiquitin-proteasome pathway and FoxO/MuRF1 gene regulation (Fisher *et al.*, 2017). Atrophy occurs following disuse and inactivity for example bed rest, casting or space flight (Phillips *et al.*, 2014; Rudrappa *et al.*, 2016; Wall *et al.*, 2015) and elevated inflammatory states/diseases such as obesity (Kalyani *et al.*, 2014), cardiac disease (Strassburg *et al.*, 2005; Von Haeling *et al.*, 2017), muscular dystrophies (Rennie *et al.*, 1982), cancer cachexia (Smith & Tisdale, 1993; Jeevanandam *et al.*, 1984), sarcopenia (aging) (Thomas, 2007) and following denervation in spinal and peripheral nerve injuries (Gorgey & Dudley, 2007).

Myofibers are long, cylindrical cells that may be many centimetres in length dependant on the specific muscle and species. Due to the large volume of cytoplasm within myofibers, homeostasis is maintained by multiple myonuclei which are dispersed along the length of the

sarcolemma of the myofiber (Bruusgaard *et al.*, 2003; Teixeira *et al.*, 2011). The traditional myonuclear domain theory suggests that as myofibers are multinucleated, each individual myonuclei governs a certain amount of cytoplasm, ensuring protein production is sufficient within its locality. A theoretical myonuclear domain upper limit also exists, therefore suggesting that for the myofiber to become larger following resistance training, additional myonuclei must be recruited from the muscles resident stem cell pool (satellite cells), in order to support the larger cytoplasmic volume. It is also well established that an increase in individual myofiber size is correlated with an increase in myonuclear number and incorporation of satellite cells into the myofiber syncytium (Allen *et al.*, 1999; Bruusgaard *et al.*, 2010; Schiaffino *et al.*, 1976; Verdijk *et al.*, 2007).

However, in the atrophic conditions mentioned above, the traditional myonuclear domain theory would suggest that during atrophy, myofibers may remove myonuclei through selective nuclear apoptosis to maintain a constant myonuclear domain size whilst transcriptomic and translational demands are reduced. Despite what the traditional model suggests, selective apoptosis of a single nucleus within a multinucleated cell has never been recorded (Gundersen, 2016). Previous work has identified that in both hindlimb suspension and denervation rodent models, atrophy is concomitant with markers of proapoptotic signalling, including elevated caspases, BAX, Apaf-1, and XIAP, using standard blotting and PCR techniques, in both predominantly slow twitch and predominantly fast twitch muscles (Alway *et al.*, 2003; Ferreira *et al.*, 2006; Siu & Alway, 2005; Siu *et al.*, 2005). However, despite the clear evidence of upregulated nuclear apoptosis in ageing and atrophy, these results are based upon muscle homogenates and are interpreted as indicating loss of myonuclei, despite the large proportion of non-myonuclei present in muscle. This is a substantial assumption to make considering that skeletal muscle also comprises various other non-myogenic tissues that make up over 50% of total nuclei in skeletal muscle (Gundersen, 2016). More recently, a study in sarcopenic mice found that only 0.8% (of 1200 counted per mouse) of myonuclei were apoptotic, whereas 46% (of 17 counted per mouse) of Pax7⁺ satellite cells were apoptotic. However, these apoptotic nuclei made up less than 20% of total apoptotic nuclei across the muscle, with the other 80% being attributed to stromal/capillary endothelial cell apoptosis (Wang *et al.*, 2014).

This highlights the importance of being able to produce a valid method of specifically identifying myonuclei when attempting to establish whether myonuclear apoptosis does in fact occur during atrophy. Immuno-histochemical approaches are most commonly employed to identify whether myonuclei are lost during atrophy, with great disparity between methodologies in identifying the myonuclei themselves and the myofiber border as well as accounting for the

thickness of cross-sections used. This has led to varying reports of myonuclear apoptosis following atrophy, with (Meneses *et al.*, 2014; Zhang *et al.*, 2010) reporting myonuclear loss when measuring nuclei per unit area of cross sections with TUNEL staining, which identifies breaks in the DNA strand through endonuclease activity. These reports were most likely attributed to the identification of non-myogenic nuclei as TUNEL binds to all broken DNA strands regardless of the lineage of the nuclei. Other cell types and their nuclei are often found in close proximity to muscle fibers including endothelial, stromal or satellite cells that lie beneath the basal lamina of myofibers. Using more stringent guidelines and considerations as to where myonuclei are present (utilising an antibody against the protein dystrophin present in the myofiber cytoskeleton), (Bruusgaard *et al.*, 2012, 2010) in contrast found no loss of myonuclei following atrophy using the definition that myonuclei lie within the geometrical centre of the dystrophin ring or on the dystrophin ring. Other studies employing the dystrophin ring staining approach have however reported loss of myonuclei following atrophy (Dupont-Versteegden *et al.*, 2006; Guo *et al.*, 2012; Oishi *et al.*, 2008; Zhu *et al.*, 2013), albeit that their reports of mean myonuclei number per control fiber on 8-10 μ m cross-sections (2.2) are much higher in comparison to that of the Gundersen group (1.7), also on 8-10 μ m sections, thus suggesting that their analysis is less stringent (Gundersen, 2016), and may incorporate capillary nuclei that often lie in close proximity to the dystrophin ring but are however distributed between myofibers.

Myofibers isolated ex-vivo following denervation have also been investigated with varying results, dependent on the method used for isolation. Whilst loss of myonuclei following denervation is reported with mechanical isolation (Viguie *et al.*, 1997) and collagenase treatments (Kawano *et al.*, 2008), extraction of single fibers via alkaline maceration has contrastingly shown no loss of myonuclei following long-term denervation (Bruusgaard *et al.*, 2010; Bruusgaard *et al.*, 2012; Wada *et al.*, 2010), potentially due to the less harsh method of extraction. Additionally, Bruusgaard and Gundersen (2008), directly observed no changes in myonuclei number following 28 days of denervation, despite total muscle volume decreasing by more than 50%, using in-vivo time-lapse imaging where specific sections of an individual muscle fiber could be followed during hind-limb suspension. Though there is clear evidence supporting nuclear loss in skeletal muscle following atrophy, there is limited evidence supporting that this nuclear loss is actually nuclei of myofibers.

Therefore, the aim of this study is to elucidate whether myonuclei are lost or gained during atrophy and recovery from atrophy using stringent methodologies to identify myonuclei outlined in (Gundersen, 2016), using samples from a previous study in rats that investigated transcriptomic/epigenetic regulation related to disuse atrophy using a TTX model (Fisher *et*

al., 2017). This model silences the nerve by reversibly blocking sodium channels, without causing nerve damage, therefore producing atrophy independent of damage/loss of motor units known to be an additional cause of fiber atrophy and subsequent loss of strength (Doherty *et al.*, 1993; Piasecki *et al.*, 2018). The hypothesis to be challenged was that we would observe 1. a significant decrease in muscle mass, anatomical cross-sectional area and individual fiber area in all TTX treated groups when compared to contralateral internal control disuse/inactivity. We also used a second model of reduction of fiber size using continuous activity by electrical stimulation at 20Hz to chronically overuse the muscle. 2. Despite significant decreases in the muscle mass, we predict that reduction in fibre size would occur independently of any changes in myonuclear number per fiber between TTX treated/20Hz electrically stimulated and the contralateral internal control limb, therefore providing evidence against the current textbook theory of myonuclear domain size following atrophy and recovery from atrophy but supporting Gundersens idea that myonuclei number is relatively stable.

Methods:

Animals:

Ethical approval was obtained, and experimental procedures were conducted with the permissions within a project licence granted under the British Home Office Animals (Scientific Procedures) Act 1986. Male Wistar rats weighing between 350-450g were housed at 20°C and 45% humidity, with food and water supplied ad libitum. Animals were assigned to 6 groups, 3 days, 7 days, 14 days, 14 days with 7 days recovery of TTX treatment, a sham control and a 20Hz 7-day electrical stimulation group ($n=6 \times 6$).

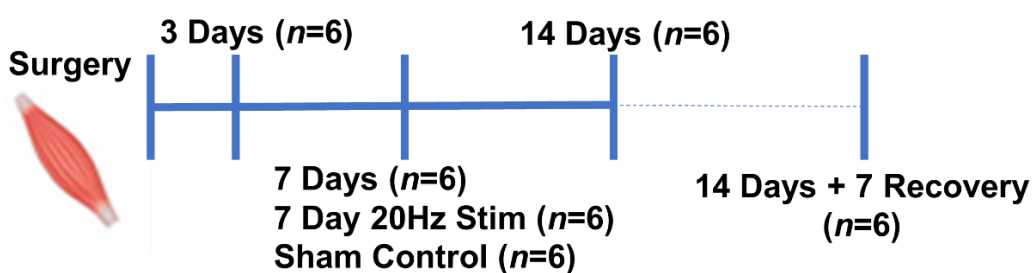


Figure 4: Schematic representation of the TTX muscle atrophy model and subsequent sampling points.

Experimental groups:

All animals were anaesthetised during implant procedures by inhalation of isoflurane, pure oxygen and nitrous oxide. Once anaesthetised, a subcutaneous injection of antibiotic (5mg/kg

Baytril®) and an intramuscular injection of Buprenorphine (0.05mg/kg Temgesic) into the right quadriceps were administered with strict asepsis kept throughout the procedure.

TTX Groups

The common peroneal nerve (CPN), the motor nerve responsible for contraction of the tibialis anterior (TA) and extensor digitorum longus (EDL) was silenced for pre-set time courses (Figure 1, outlined above via exposure to tetrodotoxin (TTX), a sodium channel blocker to induce atrophy through disuse. The electrical stimulator and osmotic pump were mounted onto biocompatible silicone rubber with Dacron mesh attached, implanted sub-cutaneously in the scapula region and sutured to the abdominal wall by way of Dacron mesh that extended from the silicone rubber to prevent migration of the implants during free-living movement. The miniosmotic pump (Mini Osmotic Pump 2002; Alzet, Cupertino, CA, USA) delivered the TTX along a delivery tube directed to a silicone rubber cuff placed around the CPN of the left hind-limb. The osmotic pump successfully delivered 0.5µl/h TTX (350mg/ml in sterile 0.9% saline) to the cuff surrounding the CPN therefore blocking ankle dorsiflexion, whilst allowing normal voluntary plantarflexion through the tibial nerve was maintained. The welfare and mobility of the rats was minimally affected during exposure. To ensure that the nerve cuff was effectively blocking nervous stimulation of the muscle, a miniature, implantable, electrical stimulator developed to deliver a fixed frequency of 20Hz which can be turned on and off remotely by a pre-programmed sequence of light flashes through the skin of the rat using a stroboscope (Jarvis & Salmons, 1991). The output electrodes were placed near to the CPN just above the blocking cuff (Fig. 2). No contraction of the muscle following 20Hz stimulation would indicate that the CPN is being appropriately blocked. For the 14-day exposure with 7-day recovery group, osmotic pumps were appropriately loaded therefore allowing for termination of TTX infusion after 14 days to allow for nerve activity to resume for 7 days of recovery via habitual physical activity. The right hind-limb was used as a contralateral control limb in all groups.

20Hz Stimulation Group

The 20Hz stimulation group received identical surgeries and implants to the TTX groups without loading of TTX into the osmotic pump. Therefore, nerve activity remained and instead the group received 20Hz of electrical stimulation for a period of 7 days to chronically overuse the muscle so that a shift to smaller fiber type occurs as previously described (Jarvis & Salmons, 1991; Jarvis *et al.*, 1996).

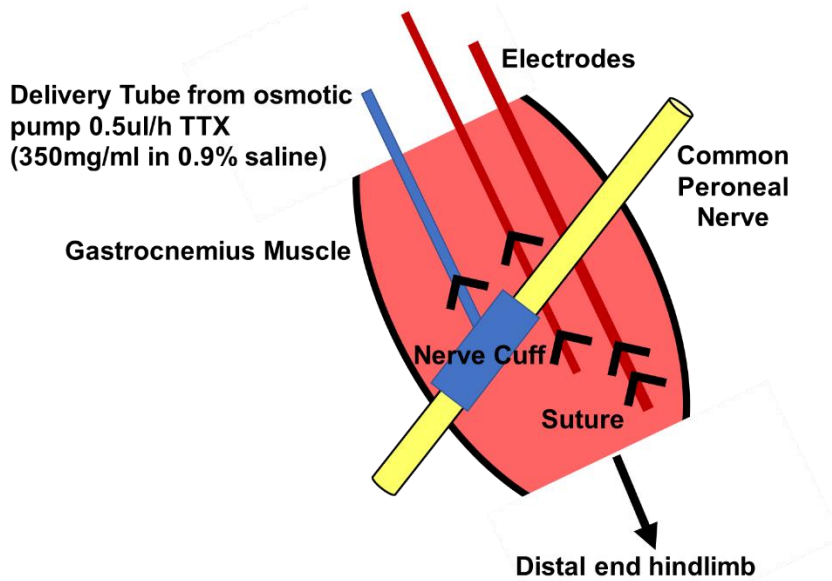


Figure 5: Schematic of Nerve Cuff and Stimulator Electrodes In-Situ

Morphology and Nuclear Density:

Preparation

After each group had finished their allocated experimental time course, animals were humanely euthanized with an increasing concentration of CO₂ and cervical dislocation. The tibialis anterior was extracted, excess connective tissue removed and weighed for assessment of muscle mass and samples taken for transcriptional analysis which has previously been reported (Fisher *et al.*, 2017). The proximal end of the muscle was frozen and fixed onto cork discs in OCT (Tissue-Tek® O.C.T. Compound, Sakura® Finetek, USA), using isopentane, pre-cooled in liquid nitrogen prior to cutting at 10µm using an OTF5000 Cryostat (Bright Instruments, UK) onto Thermo Scientific™ SuperFrost Plus™ Adhesion slides (Thermo Fisher Scientific Inc, Waltham, USA) for histological/ immunohistochemical use, to provide the sections analysed here.

Staining and Imaging

Fluorescein labelled Wheat Germ Agglutinin (WGA) staining was performed to identify changes in individual cell size and anatomical cross-sectional area (ACSA) of the muscle. WGA binds to membrane glycoproteins therefore staining all cell membranes, connective tissue and vasculature. WGA (5µl WGA (Fluorescein labeled Wheat Germ Agglutinin, Vector Laboratories Inc., Burlingame, CA, USA) per 1ml PBS) was pipetted onto thawed sections and incubated for 1 hour in the dark. 3x5 minute rinses were performed with PBS on the slide before coverslips were fixed with mounting medium containing DAPI to visualize the nuclei (Vectashield® Antifade Mounting Medium with DAPI (1.5µg/ml), Burlingame, CA, USA).

Tilescan images of the entire cross-sections were performed for WGA and DAPI using a (Leica DMB 6000, Wetzlar, Germany) and fluorescent channels overlaid (Figure 6A).

Analysis

All images were coded and then analysed by the primary researcher in a blinded manner using Image J (IBIDI, Munich, Germany) for average individual myofiber size, myofiber number, ACSA of the entire muscle and average number of myonuclei per myofiber, average individual cell size and number was performed using an automated cell counting method using Adobe Photoshop (Adobe Systems, San Jose, California, USA) and Image-Pro Plus 5.1 software (Media Cybernetics, MD, USA). Briefly, WGA only images are converted to grayscale and filtered to stylize edges in order to highlight cell membranes. Ranges of acceptance were employed to identify individual cells; (Area 500-500,000 μm^2 , minimum feret diameter 0-500,000 μm , Perimeter 0-430 μm , Roundness 0-3). This counting process is illustrated in Figure 6. ACSA was calculated from tile-scanned images of the entire muscle cross-section by tracing the outline of the cross-section using Image J (IBIDI, Munich, Germany). Average number of myonuclei per fiber (on 10 μm sections) was calculated by taking 3 random fields of view per muscle from the tilescanned image. Approximately 120-400 fibers per image were analysed depending on the state of atrophy and regional positioning of the image within the cross-section. Myonuclei were identified using adaptation of previously reported techniques (Bruusgaard *et al.*, 2010, 2012; Gunderson, 2016). Briefly, myonuclei were defined as nuclei with their geometrical center located clearly inside the myofiber membrane, combined with both nuclei found within the borders of the myofiber and nuclei with their geometrical center on the membrane of the myofiber. Myonuclear domain size was calculated by dividing the mean individual fiber cross-sectional area by the mean myonuclei number per fiber cross-section.

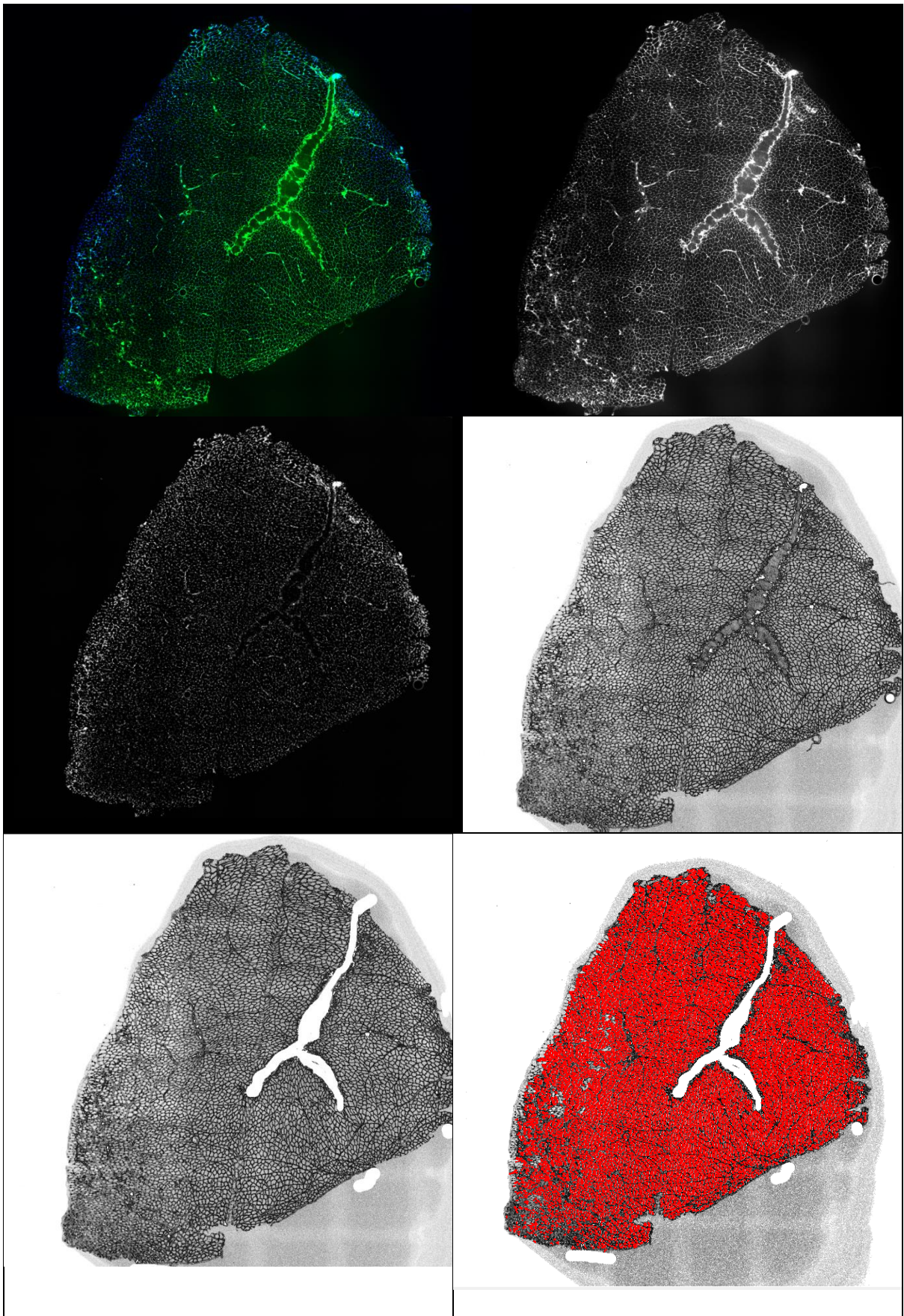




Figure 6A-G (Left to right): A=Tiles scanned, overlap image of WGA and DAPI immunostaining of a left tibialis anterior 10µm section. B=Image converted to grayscale using photoshop. C-E=Find Edges function to highlight all cell membranes, contrast/brightness enhanced followed by erasing the background and large tendons. F= Ranges of acceptance were employed to identify individual cells; (Area 500-500,000µm, minimum ferret diameter 0-500,000µm, Perimeter 0-430µm, Roundness 0-3) G=Magnified image of F, illustrating automated cell counting of myofibers and disregard for blood vessels/connective tissue.

Statistical Analyses

All statistical analyses of morphological and myonuclei data were performed using SPSS (v.24.0; SPSS, Chicago, IL, USA). Morphological (muscle mass, anatomical cross-sectional area, mean individual fiber area, fiber number and myonuclei per myofiber) comparisons between experimental and control conditions were assessed via a 1-way between-group ANOVA. Pearson's correlation was also calculated to assess co-efficient values between each morphological data set.

Results:

Muscle Mass: (Reported previously in Fisher et al., (2017), included for context.

Exposure to TTX produced an average of $7.06 \pm 2.4\%$ loss in TA muscle mass at 3 days, $28.76 \pm 5.1\%$ at 7 days, and $50.7 \pm 2.7\%$ loss after 14 days that resulted in statistical significance at all time points vs. the contralateral internal control ($P < 0.001$) and a significant difference between paired comparisons of 3 and 7 days, 3 and 14 days, 7 and 14 days ($P < 0.001$). After 14 days of TTX exposure followed by 7 days of cessation in the recovery group, muscle mass significantly recovered by 51.7% vs 14 days of TTX exposure ($P < 0.001$). Seven days of recovery did not completely restore muscle mass, as muscle mass was still significantly lower than control ($P < 0.001$) and total muscle mass was nearly equivalent to levels at 7 days of TTX administration, which suggests that rates of loss over 7 days are in

line with rates of recovery. We therefore report significant skeletal muscle atrophy of the TA muscles with disuse and significant recovery of muscle mass after 7 days of cessation of TTX administration and the return of normal habitual physical activity vs. 14 days of TTX induced inactivity of the muscle. A significant decline in muscle mass was also found for the 20Hz electrically stimulated group $12 \pm 4.84\%$ ($P < 0.002$). There was no significant reduction in muscle mass in the sham control group ($-0.133 \pm 3.79\%$, $P = 0.873$).

Muscle Anatomical Cross-Sectional Area:

Exposure to TTX produced a progressive reduction in mean muscle fiber ACSA of $6.4 \pm 6.2\%$ at 3 days, $29.75 \pm 5.1\%$ at 7 days, and $68.11 \pm 4.97\%$ at 14 days of TTX exposure, with 7 and 14 days of TTX being significantly reduced in comparison to the control limb ($P < 0.003$ and $P < 0.001$) respectively. Similarly to TA muscle mass, upon TTX cessation, the 14-day TTX + 7-day recovery group recovered muscle ACSA significantly in comparison with 14 days of TTX induced atrophy alone ($68.11 \pm 4.97\%$ vs. $24.47 \pm 9.5\%$, $P < 0.002$). A significant decline in muscle ACSA was also found for the 20Hz electrically stimulated group, $11.47 \pm 5\%$ ($P < 0.004$). There was no significant reduction in muscle ACSA in the sham control group ($0.15 \pm 1.1\%$, $P = 0.982$).

Individual Fiber Area Changes

Increasing the duration of exposure to TTX also caused a cumulative reduction in mean individual fiber size calculated through computational, automated, cell counting by $11.65 \pm 4.21\%$ at 3 days, $24.56 \pm 7.21\%$ at 7 days and $47.57 \pm 3.12\%$ after 14 days that resulted in statistical significance at all time points vs. the contralateral internal control ($P < 0.001$) and a significant difference between paired comparisons of 3 and 7 days, 3 and 14 days, 7 and 14 days ($P < 0.001$). In the 14 days TTX exposure with 7 days recovery group, mean individual fiber size was reduced by $20.82 \pm 4.1\%$ ($P < 0.001$), illustrating a recovery of fiber size by $26.75 \pm 3.1\%$ in comparison to 14 days atrophy alone ($P < 0.001$). This decrease in average fiber size and shift towards smaller atrophied fibers is outlined in a continuous format in figure 12 a-f.

Fiber Number

There was a significant percentage fiber loss after 14 days of TTX induced atrophy $-9.44 \pm 5.09\%$ ($P < 0.0001$) and 7 days of 20Hz electrical stimulation $-3.54 \pm 3.04\%$ ($P < 0.05$) in comparison to the sham control using our computational, automated, cell counting technique. There was no loss in the 3-day group $-0.26 \pm 2.84\%$ ($P = 0.635$), 7-day group $-1.15 \pm 5.06\%$ ($P = 0.383$) and 14 days with 7 days recovery group $-0.525 \pm 2.77\%$ ($P = 0.558$).

Myonuclei number per fiber cross-section

There were no significant percentage changes in myonuclei number per myofiber when compared to sham control and between limbs $-1.36 \pm 0.0219\%$ after 14 days, 0.1 ± 0.0143 after 7 days, 1.34 ± 0.0164 after 3 days and -0.6667 ± 0.0113 after 14 days with 7 days recovery ($P > 0.7$). There were also no significant percentage changes in the sham control group 1.379 ± 0.245 in comparison to the 20Hz electrical stimulation group 2.098 ± 0.215 ($P > 0.6$).

Myonuclear Domain Size Changes

There was a significant reduction in myonuclear domain size following TTX administration, $-31.32 \pm 6.34\%$ after 14 days, $-19.72 \pm 4.98\%$ after 7 days and -11.63 ± 2.35 after 3 days, all of which resulted in statistical significance at all time points vs. the contralateral internal control and percent change in the sham surgery group 3.79 ± 1.6 ($P < 0.05$). After 14 days of atrophy with 7 days recovery, myonuclear domain size had recovered to $-17.79 \pm 4.9\%$, an increase of 43.2%. A significant decline in myonuclear domain size was also found for the 20Hz electrical stimulation group of $-3.53 \pm 2.33\%$ ($P < 0.05$)

Correlations between percent changes in muscle weight, total muscle cross-sectional area, individual fiber area and myonuclear domain size changes

There was a significant positive correlation of percentage change in total muscle mass to percentage changes in distal ACSA ($R^2=0.931$, $P = 0.007$), distal individual fiber area percentage changes ($R^2=0.977$, $P = 0.001$) and the myonuclear domain size percent changes ($R^2=0.938$, $P = 0.006$). There was a significant positive correlation between ACSA percentage change and distal individual fiber area percent change ($R^2=0.924$, $P = 0.009$) and myonuclear domain size percent change ($R^2=0.838$, $P = 0.037$). There was no correlation between percentage changes in myonuclei number per myofiber and percent changes in muscle weight ($R^2=-0.92$, $P = 0.862$), muscle ACSA ($R^2=-0.263$, $P = 0.615$), and individual fiber area ($R^2=0.064$, $P = 0.904$). This illustrates there is a strong relationship between a reduction in muscle mass with loss of ACSA and individual fiber area as would be expected and these changes occur independently of myonuclear apoptosis.

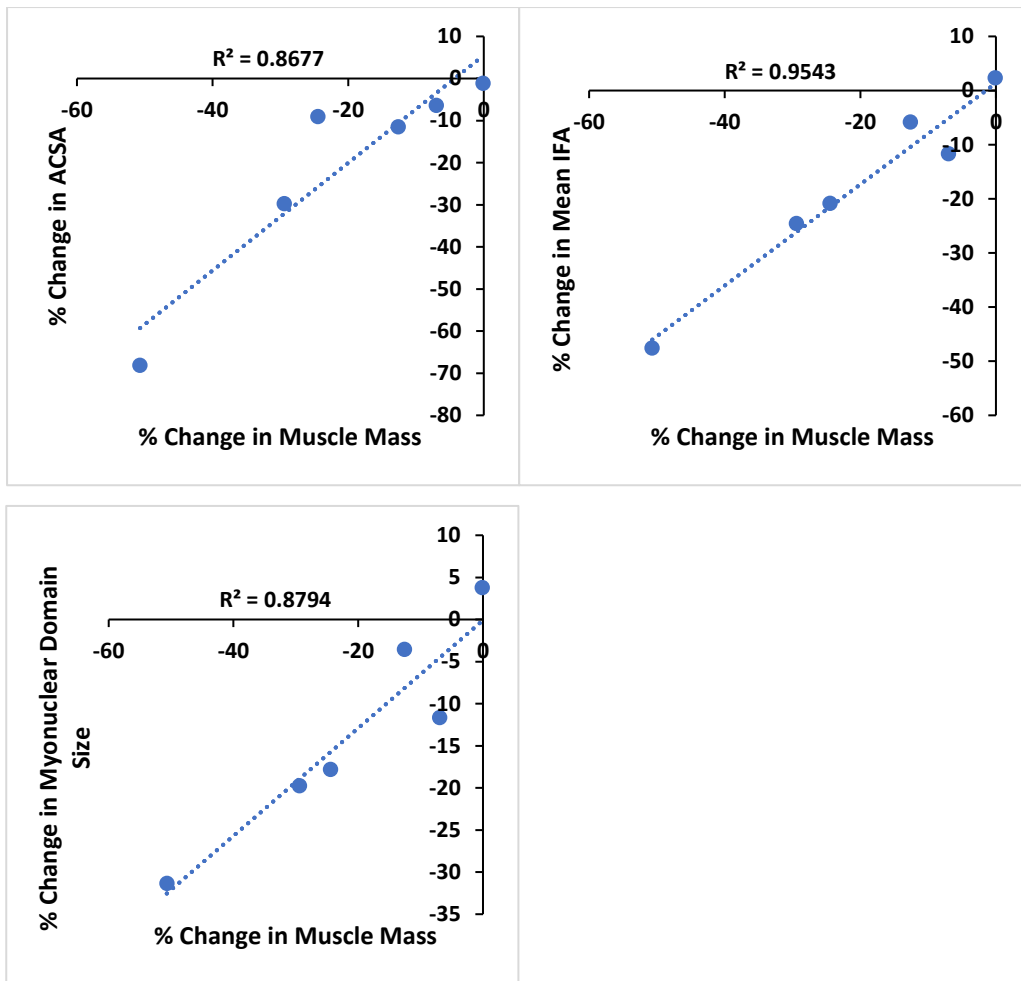


Figure 7: Correlations of % change in muscle mass to % changes in ACSA, individual fiber area and myonuclear domain size (Blue dots represent group means)

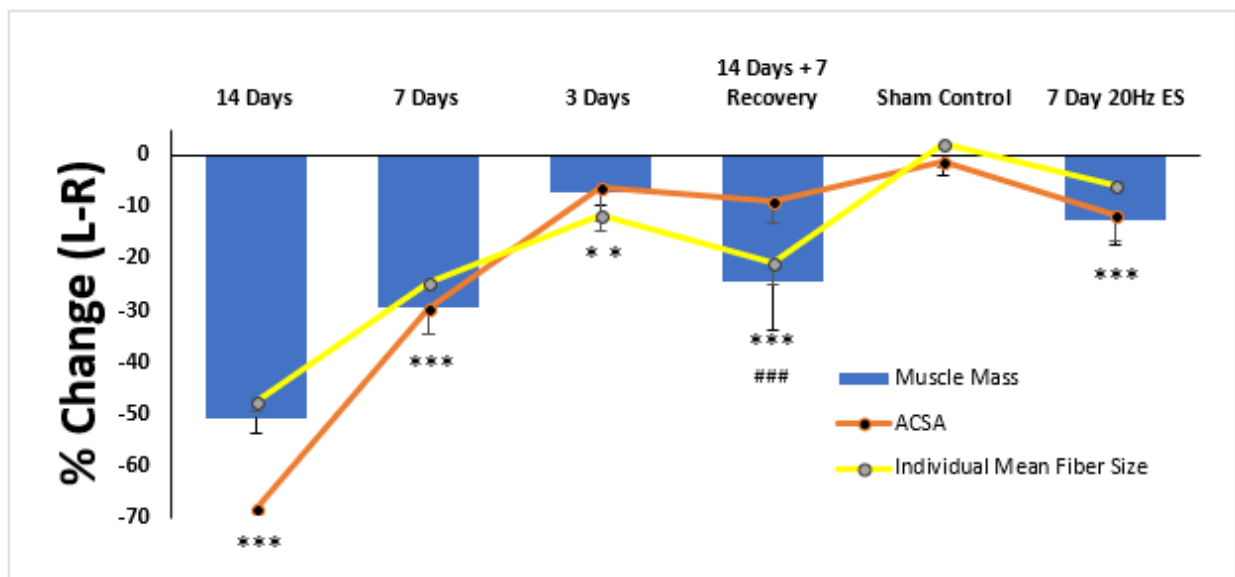


Figure 8: Changes in tibialis anterior (left as a percentage of right) muscle mass, anatomical cross-sectional area and individual mean fiber size after varying durations of TTX

administration, sham surgery and a 20Hz electrically stimulated control. *Significantly different from sham control ($p < 0.05$). # Significantly different from 14 days atrophy ($P = < 0.05$)

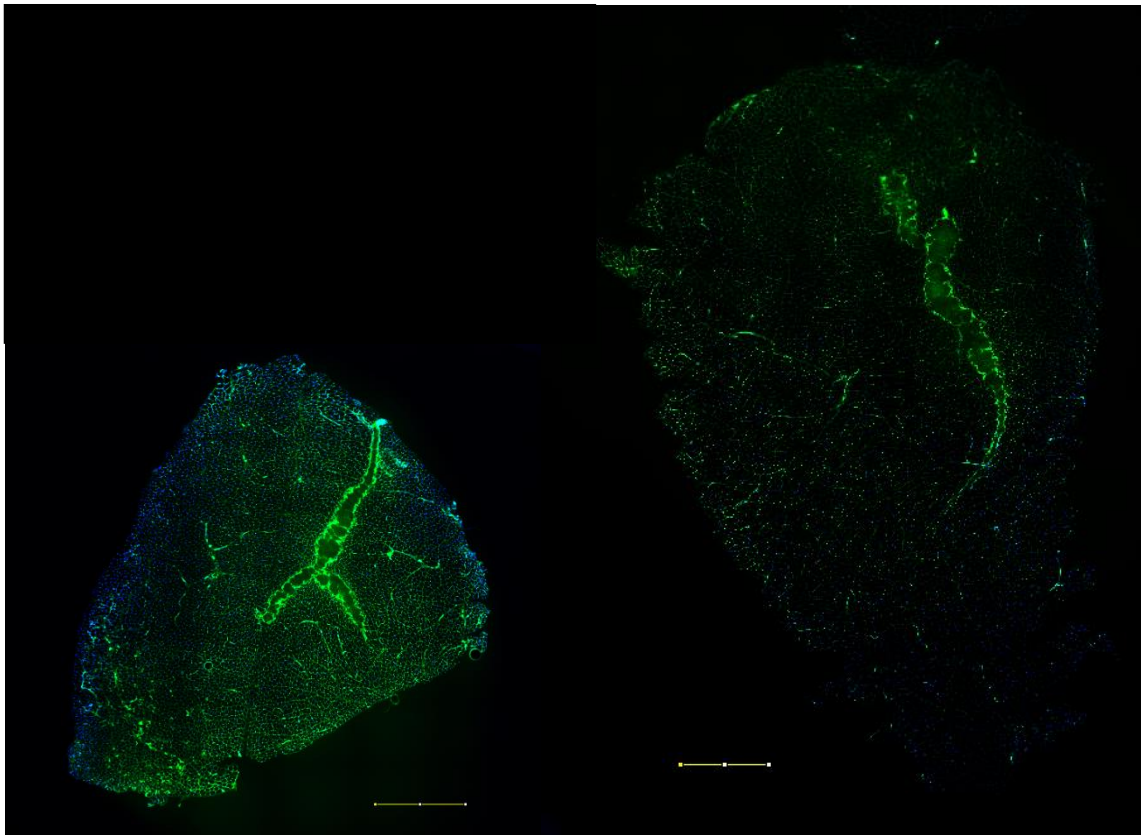


Figure 9: 14 Days TTX induced atrophy vs 14 days contralateral internal control in the tibialis anterior. Illustrates a clear loss in anatomical cross-sectional area. Scale bar = 1mm (1000 μ m).

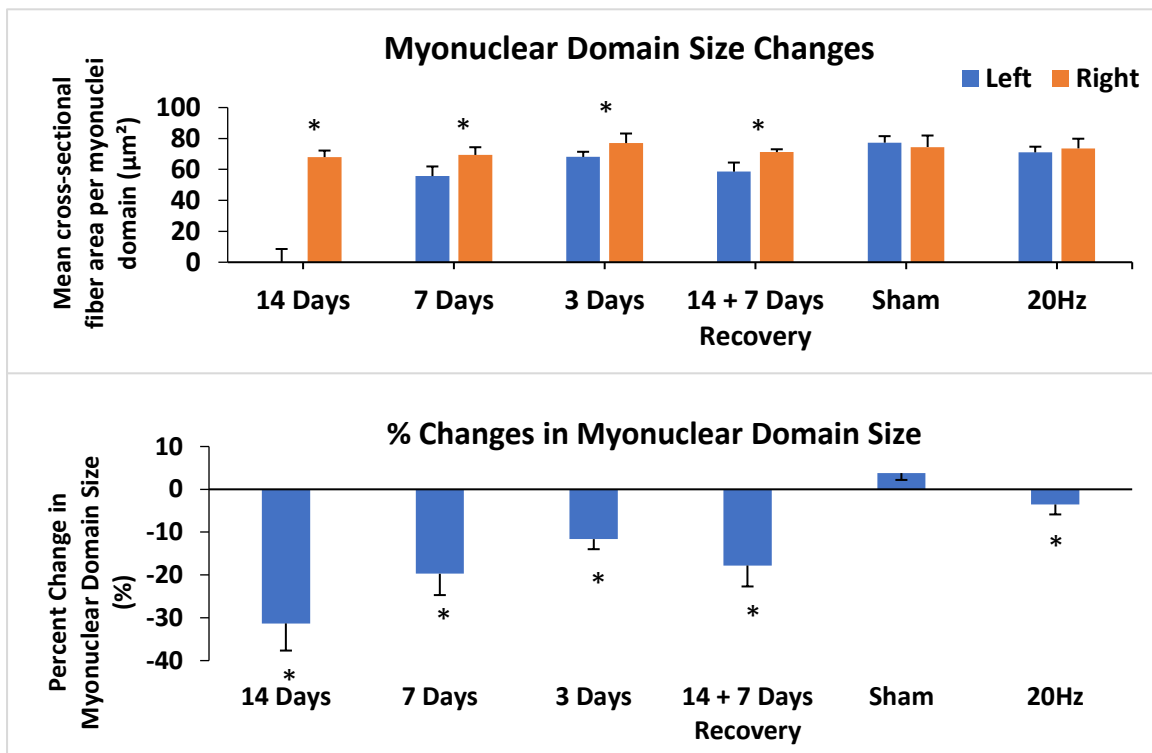


Figure 10a-b: Myonuclear Domain Size Changes presented as both mean group values, left vs. right and as percentage changes after varying durations of TTX administration, sham surgery and a 20Hz electrically stimulated control. A: * Significantly different from the contralateral internal control. B: *Significantly different from sham control ($p < 0.05$).

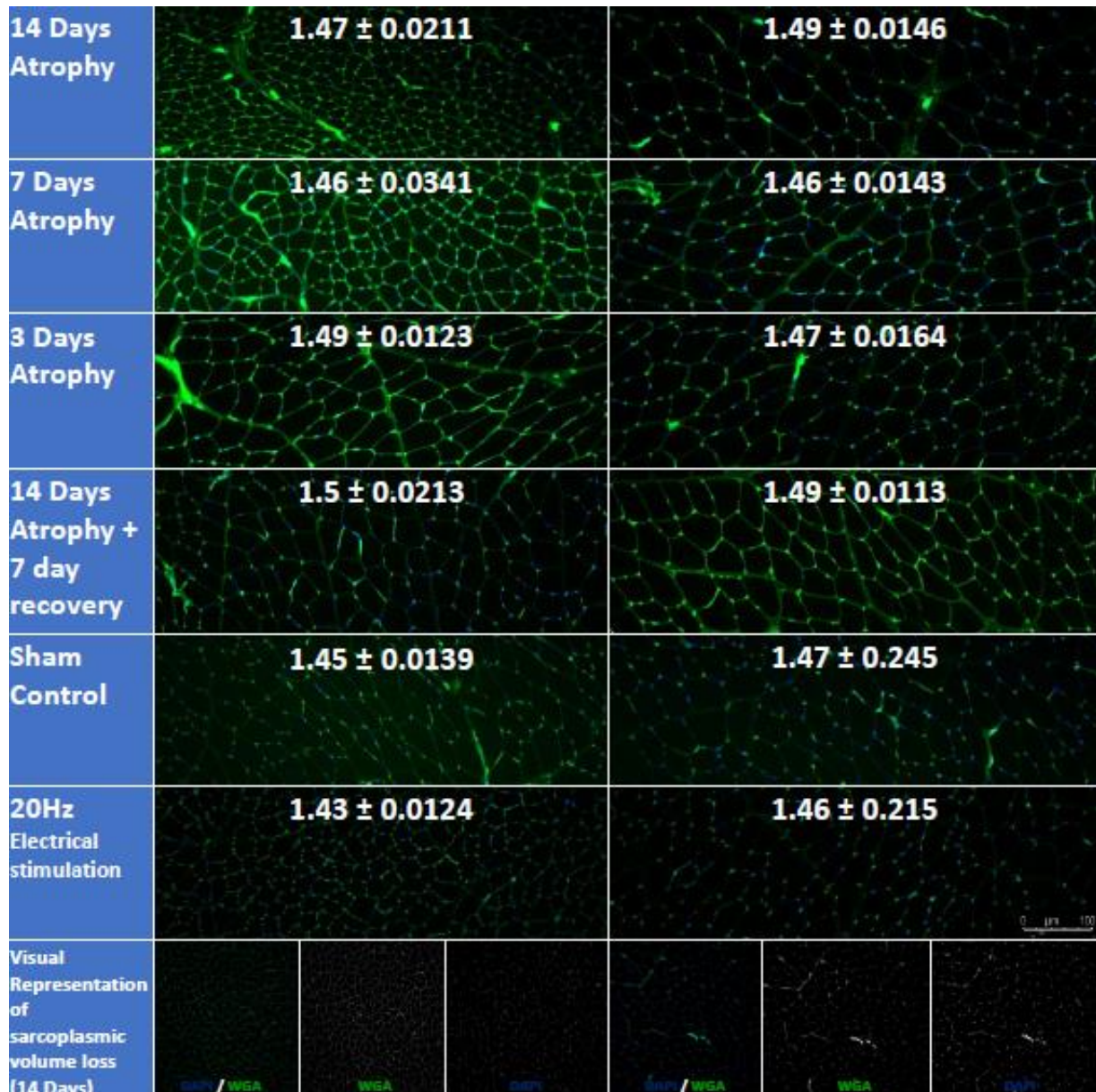
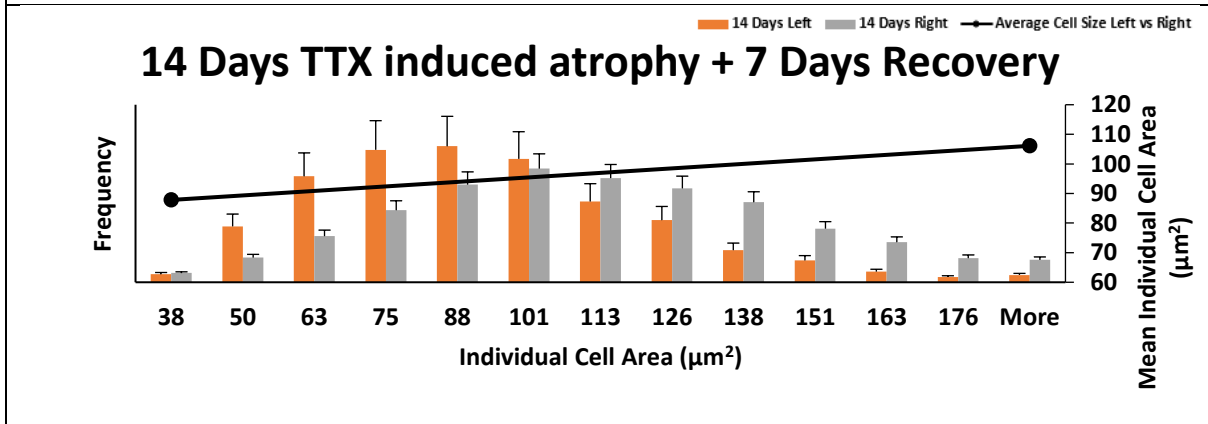
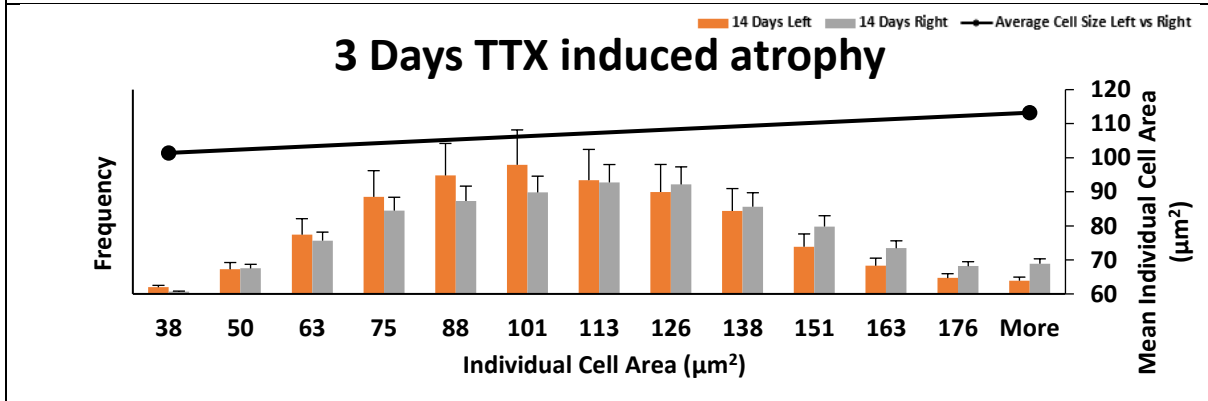
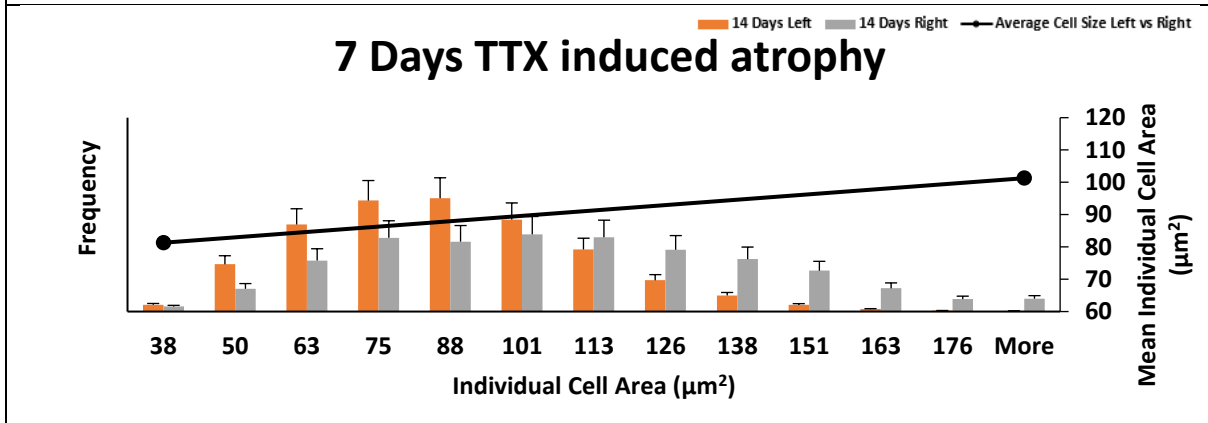
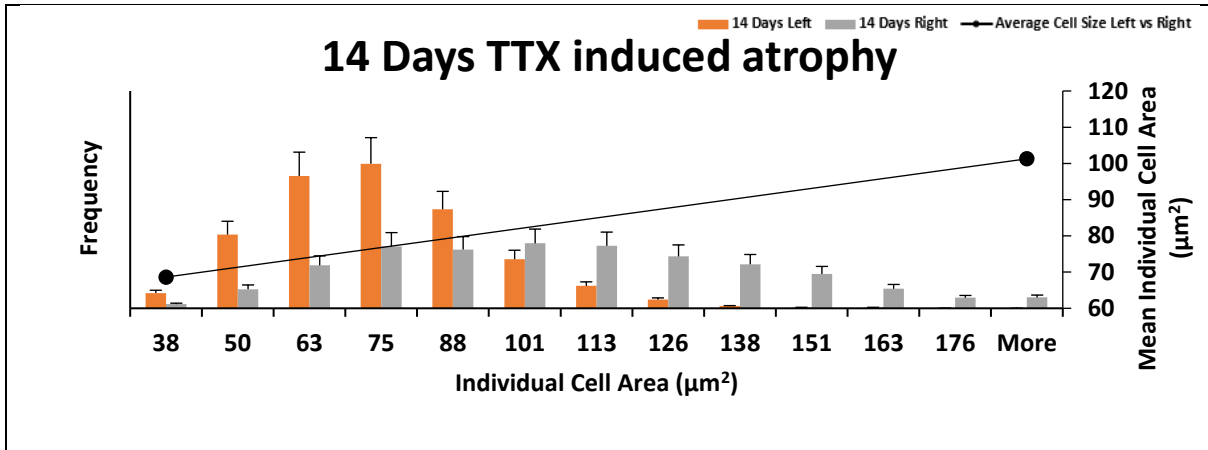


Figure 11: Comparison of mean myonuclei counts between limbs across varying time courses with accompanying WGA/DAPI images.



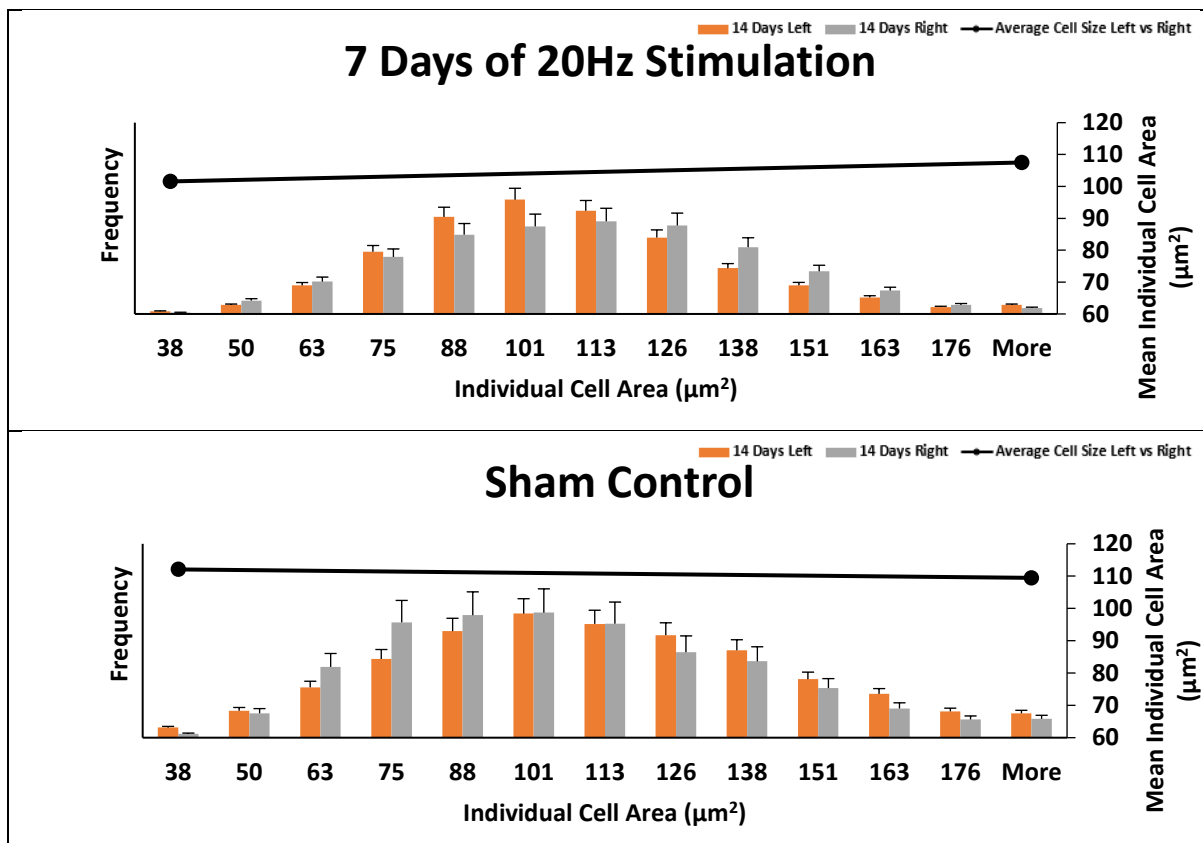


Figure 12a-f: Individual Cell Area ($\times F_{\min \text{ diameter}} \times \pi$) frequency experimental (orange) vs. control (grey).
An orange shift to the left illustrates a loss in fiber size in the TTX treated limb. Mean left vs right individual cell area is illustrated with a line graph.

Discussion:

Summary:

The aim of this study was to produce TTX induced atrophy in the tibialis anterior muscle of the left hindlimb, after varying durations of TTX treatment, to elucidate the rate at which the tibialis anterior muscle atrophies in response to disuse/inactivity and whether myonuclear number per fiber is altered as a result of a reduction in domain volume. The hypothesis to be tested was that we would observe 1. a significant decrease in muscle mass, ACSA and individual fiber area in all TTX treated groups when compared to contralateral internal controls through disuse/inactivity. 2. Despite significant decreases in morphology, we hypothesised that decreases in the mass and cross-sectional area of the muscle would occur independently of any changes in myonuclear number per fiber between TTX treated and the contralateral internal control limb. 3, The 7-day 20Hz electrical stimulation group model would also produce significant atrophy to the tibialis anterior via overuse, in comparison to the contralateral internal control limb and the loss in muscle mass, ACSA and individual fiber area would occur independently of changes in myonuclei number per fiber. Previous models of the myonuclear

domain theory have suggested that when myofibers hypertrophy, myonuclei are recruited into the syncytium of myofibers from satellite cells to help support the larger cytoplasmic volume. Following atrophy, when cytoplasmic volume decreases, excess myonuclei are removed through apoptosis.

Through TTX exposure to the CPN, therefore blocking TA contraction, we demonstrated that we could cause considerable significant skeletal muscle atrophy in the tibialis anterior of the rat. The significant loss of muscle mass of $50.7 \pm 2.7\%$ ($P < 0.0001$) after 14 days of exposure was concomitant with a loss in anatomical cross-sectional area $68.11 \pm 4.97\%$ ($P < 0.003$) and the average cell size 47.57 ± 3.12 ($P < 0.001$) when compared to the contralateral internal control limb, as expected with the loss of sarcoplasmic volume and myofibrillar proteins (Wilkinson *et al*, 2018). This represents changes in muscle size that are well beyond most exercise-related changes in human subjects. These findings displayed high correlation coefficients with R^2 achieving a minimum of 0.93 between muscle weight, ACSA and individual mean fiber area.

Using stringent immunohistochemistry technique guidelines adapted from Gundersen (2016), we were able to establish that myonuclear number per myofiber cross section did not change significantly alter across all treated muscles between treated limbs and internal control limbs studied and this showed no correlation across any time points with muscle mass, ACSA and individual fiber area. This provides evidence of the remarkable capability of skeletal muscle to maintain its myonuclei number despite considerable atrophy, albeit occurring over a short period in this study. Due to this maintenance, following subsequent recovery from atrophy, ACSA, individual fiber area and muscle weight all recovered substantially, occurring independently of any change in myonuclei number. This provides evidence that adult rodent skeletal muscle can hypertrophy following return to activity to its normal state, without the need for incorporation of satellite cells into the myofiber syncytium, as there is already a substantial number of myonuclei available to maintain the cytoplasmic volume.

Limited evidence for hypoplasia during atrophy and hyperplasia during recovery:

Whilst our automated cell counting data indicated that after 14 days of TTX induced atrophy significant fiber loss had occurred ($-9.44 \pm 5.09\%$), our histological analysis showed no evidence of degrading fibers. There was also no significant evidence of hypoplasia/hyperplasia in the 3 or 7 days of TTX administration. Additionally, after 14 days with 7 days recovery, fiber number had appeared to have recovered to that of the sham control. However, there was no evidence of hyperplasia (centralised nuclei) in any of the histology sections, signifying that if hyperplasia had occurred, our time point of extraction was too late to observe this occurring. Instead, we believe variations in fiber number are more likely due to measurement error in our automated counting methodology (extremely small atrophied fibers

not counted in our inclusion criteria that could not be distinguished between connective tissues if this were the case), in addition to cross-section quality and distance cut from the myotendinous junction. Another consideration must be that due to the considerable atrophy, the shape of the muscle changed meaning that the atrophied muscles were analysed nearer to the end of the muscle and therefore naturally contained slightly fewer fibers. Supporting this, whilst it is established that ageing can cause fiber loss as a result of loss of motor units and denervation (Frontera *et al.*, 2000; Lexell *et al.*, 1988; Spendiff *et al.*, 2016; McPhee *et al.*, 2018), as far as we are aware, there is no evidence of fiber loss (hypoplasia) following short term disuse atrophy. There is also no evidence of skeletal muscle hyperplasia occurring following return to normal, habitual, physical activity following hind-limb suspension, exposure to microgravity and TTX administration studies in rodents nor bedrest or limb immobilisation studies in humans. The novelty of our model also ensures that nerve damage does not occur, instead the nerve is simply silenced therefore preserving motor units, unlike the atrophy/hypoplasia occurring in sarcopenia (Fisher *et al.*, 2017). Despite evidence suggesting that various forms of mechanical loading can produce a $15 \pm 19.60\%$ increase in number of fibers (Kelley, 1996), this is species specific (avian, 20.95%, and mammalian, 7.97% increases). Furthermore, previous animal work (Sola *et al.*, 1973) has suggested that skeletal muscle hyperplasia occurs following mechanical stretch as a function of both the amount of stretch, length of chronic training and the amount of hypertrophy, with 'de-novo' fibers only being added after approximately 70% hypertrophy of the original muscle size. As neither of our groups had undergone extensive stretching/mechanical load or hypertrophied to the extent that splitting of existing fibers may occur, we believe that the likelihood of hyperplasia attributing to the recovery of the muscle following atrophy is unlikely to occur. We believe it represents increases in individual cell size and protein content, rather than increase in fiber number, in line with our automated cell counting results.

Are removal and recruitment of myonuclei obligatory for atrophy and recovery from atrophy?

Briefly, using our method of identification for myonuclei we observed no significant changes in myonuclei number after 2 weeks between atrophied muscles and control muscles or between any groups of TTX administration or electrical stimulation. These results suggest that skeletal muscle atrophy and the ensuing recovery from atrophy following disuse, is in part controlled by the remarkable capability of the existing nuclear population to adequately control substantial changes in the sarcoplasmic volume of their myonuclear domains in the short term, in order to support retrieval of normal, healthy muscle mass. However, we cannot confirm that this is the case in longer periods of atrophy. In terms of the rate at which the tibialis anterior atrophied, previous studies employing TTX administration to induce paralysis and subsequent

atrophy observed similar levels of atrophy in the tibialis anterior, confirmed by measurements of both loss in muscle mass and individual fiber area at both 7 days ($19 \pm 5\%$, $26 \pm 14\%$ and 14 days ($39 \pm 10\%$, $45 \pm 5\%$) (Gardiner *et al.*, 1992; Salter *et al.*, 2003). Whilst our analysis did not include isoform specific losses in fiber cross-sectional area, previous studies have shown that in the tibialis anterior, a predominantly fast twitch muscle (98%), type IIa fibers ($29 \pm 10\%$ loss) appeared to atrophy less than type IIb fibers ($43 \pm 7\%$ loss) after a period of 1-week (Salter *et al.*, 2003); potentially through an evolutionary mechanism and natural selection, whereby type IIb fibers atrophy quicker than their oxidative counterparts. This may be to help preserve more mitochondria found in type IIa fibers, and to eliminate the cost of having more contractile proteins and ATPase activity in the type IIb fibers (Pette & Staron, 2001). Type II muscle fibers have also been found to undergo extensive atrophy in elderly hip fracture patients, to a greater extent than type I fibers in the vastus lateralis (a mixed fiber muscle, Staron *et al.*, 2000) (Kramer *et al.*, 2017). As we have established, the reduction in fiber size and mass following disuse happens independently of myonuclei loss, therefore proposing that this gives muscle a mechanism whereby following atrophy/periods of net protein degradation, cytoplasmic contents can be quickly removed and on the other hand, in periods of activity and net protein synthesis, muscle can quickly restore protein content and contractile units, without the need for recruiting new myonuclei into the syncytium. Subsequently following recovery from the TTX induced atrophy as the muscle hypertrophies, our results provide further evidence that adult skeletal muscle can hypertrophy (51.7% muscle mass, 43.6% ACSA and 26.75% individual fiber area increases after 7 days recovery), without the recruitment of myonuclei into the myofiber syncytium, at least when returning to 'normal size'. Our results share similarities with (Jackson *et al.*, 2012) who reported radial growth of cross-sectional area of up to 60% following 2 weeks of reloading via normal, habitual, physical activity in a hind-limb suspension model, using a satellite cell knockout mouse.

Despite the large amount of atrophy we produced after 2 weeks of TTX administration, it is clear that this did not cause complete removal of fibers or apoptosis of any myonuclei unlike that found in disease states such as sarcopenia following denervation (Cheema *et al.*, 2015) and damage to the sarcolemma following contraction in muscular dystrophies (Campbell, 1995). Thus we are suggesting that only when muscle cannot adapt to the environment through control of the phenotype, in the case of chronic loading (Kadi *et al.*, 2000; 2005) and extreme damage (Murphy *et al.*, 2011), then the muscles resident stem cells, the satellite cell will become activated and fuse with current myofibers to aid in growth, or satellite cells will fuse together to produce 'de-novo' fibers in extreme inflammatory or overload circumstances (You *et al.*, 2018). Although satellite cell activation was not measured in this study, one would expect a subsequent increase in myonuclei number per fibre cross-section if satellite cells were in fact activating, proliferating and fusing to myofibers during the recovery from atrophy.

Further evidence supporting this theory has shown that following overload-induced growth (synergist ablation), hypertrophic adaptation continues in the absence of satellite cells in fully grown Pax7- DTA adult mice but is severely blunted or stopped completely in neonatal Pax7- DTA mouse growth, where the mean myonuclei per fiber is lower and therefore cannot grow to the same extent without new myonuclei (Murach *et al.*, 2017). Whilst some studies show activation and proliferation of satellite cells during hypertrophy without integration into existing fibers, this may be more related to the remodelling of the extracellular matrix and controlling fibroblasts if the cytoplasmic volume is controllable by the myonuclear density (Murphy *et al.*, 2011).

This provides evidence supporting the hypothesis that there may be a ceiling effect whereby there is a limit to which a myonuclei can control a given amount of cytoplasm and therefore a limit to cell hypertrophy, after which there is signalling cascade to trigger recruitment of satellite cells into myofiber if satellite cells are not present, as is the case in Pax7-DTA mice, growth will not occur (Murphy *et al.*, 2011). (Kadi *et al.*, 2005; Petrella *et al.*, 2006, 2008) has previously reported that the limit to hypertrophy without triggering recruitment of myonuclei is between 17-36%. Whilst these reports have often been made in regard to the limit following strength training, the muscle in fact has the potential to hypertrophy more than what has previously been indicated without the aid of satellite cells, if the muscle is atrophied and possesses a low myonuclear domain size. This contributes to the theory proposed by Gundersen (2016), that muscle has a cellular memory of training history, through maintaining any myonuclear accretion even during periods of atrophy. To test this further (Bruusgaard *et al.*, (2010) and Egner *et al.*, (2013) have previously produced hypertrophy and myonuclear accretion in a mouse model, via a 2-week pre-treatment with testosterone. This hormone drives an increase in protein synthesis through IGF-1 and downstream mTOR/p70s6k signalling (Basualto-Alarcón *et al.*, 2013) and satellite cell activation/fusion to myofibers (Joubert & Tobin, 1995; Sinha-Hikim *et al.*, 2003). After 3 weeks of withdrawal of testosterone, myofiber size had returned to normal but myonuclei number was still elevated. When this group was subjected to overload, those with pre-treatment of testosterone grew by 36% in 2-weeks in comparison to only 6% in the sham control, again demonstrating the extraordinary ability of myonuclei to act as a protective mechanism when muscle must quickly adapt. Whilst this is a supraphysiological approach to promote fiber enlargement alongside incorporation of satellite cells within the muscle, further investigations must be made using resistance training/nutritional intervention to elucidate whether the same occurs as in the above testosterone study; similarly to the design used in the epigenetic study of muscle hypertrophy, Seaborne *et al.*, (2018).

Whilst epigenetic alterations have been shown to aid in hypertrophy Seaborne *et al.*, (2018), our study amongst others has provided evidence of a myonuclear memory through the

maintenance of myonuclear number per fiber cross-section during atrophy and recovery from atrophy. Though atrophy leads to small fibers with a high nuclear density and a small myonuclear domain, the muscle is able to recover without recruitment of new myonuclei allowing for an efficient growth period until myonuclear density becomes incapable of maintaining the cytoplasmic volume.

Limitations:

Whilst our analysis followed stringent guidelines and methodologies outlined previously by Gundersen (2016) and adapted further still, there are still clear potential discrepancies between techniques for identifying and counting myonuclei in histology/immunohistochemical cross sections which has probably contributed to differences reported in myonuclei number at both an intra and inter species level. Whilst we are confident that our method removes the counting of non-myonuclei in surrounding connective tissues and capillaries we cannot rule out the possible false reporting of satellite cells in our myonuclei count and other non-myonuclei. However, the range of myonuclei per fiber cross-section in our analysis ranged from 1.43-1.51 which is lower than that reported in other immunohistochemical atrophy studies using a dystrophin ring technique (1.7-3.15) (Gundersen, 2016), suggesting that our inclusion criteria for myonuclei was more rigorous or that our cross-sections were slightly thinner. Since the original analysis in this study, a study from the Gundersen group has identified and validated the use of the antibody against Pericentriolar material 1 (PCM1) to identify nuclei specific to myogenic lineage without binding to satellite cell, allowing us to elucidate basic biological processes involved in myonuclear domain size changes in response to atrophy and hypertrophy (Brunn, 2018; Murach *et al.*, 2018; Winje *et al.*, 2018). The gene itself encoding the PCM1 228-kD centrosome protein is responsible for cytoskeleton organisation, nucleation and anchoring of microtubules and has also been shown to be pivotal for the subsarcolemmal positioning of myonuclei in myofibers (Espigat-Georger *et al.*, 2016; Gimpel *et al.*, 2017). The marker itself is confined to the nuclear membrane of all cells in interphase of the cell cycle, irrespective of cell lineage. As myonuclei do not undergo mitosis and myogenesis is controlled by satellite cells within skeletal muscle, this marker provides a useful discrimination between myonuclei and non-myonuclei, and therefore, should become standard practice in any skeletal muscle research relating to the myonuclear domain.

Conclusion:

Whilst the original work from our group (Fisher *et al.* 2017) has provided evidence that skeletal muscle disuse atrophy is associated with reversible epigenetic alterations of the transcriptome, allowing for recovery of gene expression in recovery from atrophy back to the muscles original state, regarded as an 'epi-memory' (Seaborne *et al.*, 2018; Sharples *et al.*,

2016), work from the Gundersen group and from this study clearly illustrate the potential for skeletal muscle to also possess a cellular memory of its original size and training history prior to atrophying, due to the durability of myonuclei. This would suggest that further therapeutic research should not be concentrated on recruitment of satellite cells into the syncytium, nor blocking of apoptotic pathways, but instead should concentrate on the promotion of protein synthesis and reduction of protein degradation within the muscle. We cannot however rule out that myonuclei apoptosis does not occur after longer periods of disuse atrophy. We therefore propose to further test this hypothesis by adding additional groups to this study to observe atrophy over a longer time course. Additionally, using our co-activation model of electrical stimulation (Schmoll *et al.*, 2017), we propose to chronically train Wistar rats, to stimulate hypertrophy and remodelling of the myofiber to stimulate incorporation of satellite cells into the myofiber to increase the myonuclei number per fiber. Following this, we would produce atrophy within different groups to establish the time course relationship between trained and untrained muscle atrophy and recovery following atrophy, as well as any potential changes in myonuclei number using the most valid methods of identification (anti-PCM1/dystrophin ring labelling).

Chapter 5: Future Directions for PhD study

Adequate muscle strength is a major factor in maintaining mobility and independent living, and thus a key focus of research in healthy ageing across the globe. Allied Health professionals have a key role in enhancing the quality of life in older years, but they need effective means to enhance muscle strength and endurance. Resistance training exercise generates mechanical stimuli within muscles that trigger adaptive cellular responses. Typically, muscle fibres grow by hypertrophy (an accumulation of myofibrillar proteins that increases muscle cross sectional area and strength). The cellular level responses lead to larger total skeletal muscle mass and quality which contributes significantly to prevention of morbidity and is associated with higher quality of life in the elderly. The adaptation and regeneration of skeletal muscle involves the activation of satellite cells (the resident muscle stem cell), and the mechanistic target of rapamycin (mTOR) signaling pathway, which centrally regulates mammalian cell growth, metabolism and survival. We know that mechanical signaling significantly activates mTOR pathways and that mTOR activation alone can induce hypertrophy. But our knowledge of how these mechanical stimuli are converted into biochemical events that induce cell growth and hypertrophy is extremely limited.

Recently, several respected scientists have published papers investigating the intracellular movement and co-localisation of mTOR with other signaling proteins, such as lysosomal proteins and tuberous sclerosis complex 2 (TSC2) following mechanical stimuli. Once these mechanisms are better understood, there may be opportunities to enhance the hypertrophic response and to reduce the atrophic response by identifying targets that are protective of muscle mass and degeneration. (Jacobs *et al.*, 2013, Song *et al.*, 2017).

Although this research is highly respected, there are key limitations that we can overcome with new techniques included in this thesis and from previous work from within the research group (Fisher *et al.*, 2017; Schmoll *et al.*, 2017). Studies in competing laboratories tend to use just one bout of muscle activation under anesthesia to investigate translocation of mTOR and protein complex localisation following mechanical stimuli. This is also only assessed at the mid-belly level of one muscle. To translate this work to a stage at which it is applicable to the complexity of mammalian musculature that undergoes many mechanical stimuli per day, we will use a novel, surgically implanted, programmable electrical stimulator in our rodent model to produce mechanical stimuli in the lower limb with control over intensity, duration per day and length in days or weeks of the prescribed exercise regime. Moreover, we can limit programmed exercise to one limb, so that the contralateral limb serves as an essential control. We have established a programme of well-tolerated resisted exercise by co-contraction (one set of muscles working against another) that can generate consistent hypertrophy of about

15% with two 20-minute programmed sessions per day. We will investigate the time course of the response and underlying mechanisms of adaptation, harvesting muscles at 2 days, 7 days and 28 days of exercise, and investigate the markers of over-stimulation by increasing the numbers of sessions per day from 2 to 6.

Through immunofluorescence, confocal microscopy and flow cytometry techniques developed in this thesis, we will measure regional changes and muscle group differences, to pinpoint where mechanical stimuli are regulating mTOR signaling and why some muscle groups are deficient in mTOR related signaling proteins and are therefore susceptible to atrophy (loss of muscle mass/degeneration). With methods developed during this year of my study, we can now complete morphological analysis of whole muscle cross-sections of the proximal, mid-belly and distal parts of the muscle with computational image analysis. We can thus investigate regional differences in mTOR translocation and protein complex co-localisation, as well as changes in morphology, myonuclei number and satellite cell behaviour, alongside continued development of quantitative individual fiber type/isoform specific protein phosphorylation via flow cytometry.

By understanding the intricate mechanisms underpinning skeletal muscle hypertrophy and atrophy, we will also inform the practical use of electrical stimulation to generate assisted exercise in human clinical and rehabilitation settings, with our collaborators at the University of Vienna and the Swiss Paraplegic Centre Nottwil. This research will ultimately show how muscle mass is increased through the transfer of mechanical stimuli into molecular level, biochemical changes in mTOR signaling. Identifying and understanding these mechanisms is critical to inform future research on interventions that attempt to capitalise on the potency of mechanical stimuli for use in clinical settings, to reverse or prevent the loss of muscle associated with obesity, cardiac disease, muscular dystrophies, cancer cachexia and ageing. This is particularly important when heavy resistance exercise is not safe or feasible and therefore alternative interventions are required.

References:

Adams, J.D., Kim, U. and Soh, H.T., (2008). Multitarget magnetic activated cell sorter. *Proceedings of the National Academy of Sciences*, 105(47), 18165-18170.

Aldridge, G.M., Podrebarac, D.M., Greenough, W.T. and Weiler, I.J., (2008). The use of total protein stains as loading controls: an alternative to high-abundance single-protein controls in semi-quantitative immunoblotting. *Journal of neuroscience methods*, 172(2), 250-254.

Alway, S.E., Degens, H., Krishnamurthy, G. and Chaudhrai, A., (2003). Denervation stimulates apoptosis but not Id2 expression in hindlimb muscles of aged rats. *The Journals of Gerontology Series A: Biological Sciences and Medical Sciences*, 58(8), 687-697.

Antonio, J. and Gonyea, W.J., (1993). Progressive stretch overload of skeletal muscle results in hypertrophy before hyperplasia. *Journal Of Applied Physiology*, 75(3), 1263-1271.

Antonio, J. and Gonyea, W.J., 1994. Muscle fiber splitting in stretch-enlarged avian muscle. *Medicine and science in sports and exercise*, 26(8), 973-977.

Areta, J.L., Burke, L.M., Camera, D.M., West, D.W., Crawshay, S., Moore, D.R., Stellingwerff, T., Phillips, S.M., Hawley, J.A. and Coffey, V.G., (2014). Reduced resting skeletal muscle protein synthesis is rescued by resistance exercise and protein ingestion following short-term energy deficit. *American Journal of Physiology-Endocrinology and Metabolism*, 306(8), 989-997.

Armstrong, R. B., Ogilvie, R. W., & Schwane, J. A. (1983). Eccentric exercise-induced injury to rat skeletal muscle. *Journal of Applied Physiology*, 70, 80 – 93.

Arnold, H.H. and Braun, T., (2003). Targeted inactivation of myogenic factor genes reveals their role during mouse myogenesis: a review. *International Journal of Developmental Biology*, 40(1), 345-353.

Baar, K. and Esser, K., (1999). Phosphorylation of p70S6 correlates with increased skeletal muscle mass following resistance exercise. *American Journal of Physiology-Cell Physiology*, 276(1), C120-C127.

Bass, J.J., Wilkinson, D.J., Rankin, D., Phillips, B.E., Szewczyk, N.J., Smith, K. and Atherton, P.J., (2017). An overview of technical considerations for Western blotting applications to physiological research. *Scandinavian journal of medicine & science in sports*, 27(1), 4-25.

Billin, A.N., Bantscheff, M., Drewes, G., Ghidelli-Disse, S., Holt, J.A., Kramer, H.F., McDougal, A.J., and Smalley, T.L., (2016). Discovery of novel small molecules that activate satellite cell proliferation and enhance repair of damaged muscle. *ACS Chemical Biology*, 11(2), 518-529.

Bodine, S.C., Stitt, T.N., Gonzalez, M., Kline, W.O., Stover, G.L., Bauerlein, R., Zlotchenko, E., Scrimgeour, A., Lawrence, J.C., Glass, D.J. and Yancopoulos, G.D., (2001). Akt/mTOR pathway is a crucial regulator of skeletal muscle hypertrophy and can prevent muscle atrophy in vivo. *Nature cell biology*, 3(11), 1014.

Bolster, D.R., Crozier, S.J., Kimball, S.R. and Jefferson, L.S., (2002). AMP-activated protein kinase suppresses protein synthesis in rat skeletal muscle through down-regulated mammalian target of rapamycin (mTOR) signaling. *Journal of Biological Chemistry*, 277(27), 23977-23980.

Brook, M.S., Wilkinson, D.J., Mitchell, W.K., Lund, J.N., Szewczyk, N.J., Greenhaff, P.L., Smith, K. and Atherton, P.J., (2015). Skeletal muscle hypertrophy adaptations predominate in the early stages of resistance exercise training, matching deuterium oxide-derived measures of muscle protein synthesis and mechanistic target of rapamycin complex 1 signaling. *The FASEB Journal*, 29(11), 4485-4496.

Brook, M.S., Wilkinson, D.J., Mitchell, W.K., Lund, J.L., Phillips, B.E., Szewczyk, N.J., Kainulainen, H., Lensu, S., Koch, L.G., Britton, S.L. and Greenhaff, P.L., (2017). A novel D2O tracer method to quantify RNA turnover as a biomarker of de novo ribosomal biogenesis, in vitro, in animal models, and in human skeletal muscle. *American Journal of Physiology-Endocrinology and Metabolism*, 313(6), 681-689.

Brown EJ, Albers MW, Shin TB, Ichikawa K, Keith CT, Lane WS, Schreiber SL (1994). A mammalian protein targeted by G1-arresting rapamycin-receptor complex. *Nature*. 369 (6483): 756–8.

Brunn, A., (2018). The complex pericentriolar material 1 protein allows differentiation between myonuclei and nuclei of satellite cells of the skeletal muscle. *Acta Physiologica*, 13103.

Bruusgaard, J.C., Liestøl, K., Ekmark, M., Kollstad, K. and Gundersen, K., (2003). Number and spatial distribution of nuclei in the muscle fibres of normal mice studied in vivo. *The Journal of physiology*, 551(2), 467-478.

Bruusgaard, J.C. and Gundersen, K., (2008). In vivo time-lapse microscopy reveals no loss of murine myonuclei during weeks of muscle atrophy. *The Journal of clinical investigation*, 118(4), 1450-1457.

Bruusgaard, J.C., Johansen, I.B., Egner, I.M., Rana, Z.A. and Gundersen, K., (2010). Myonuclei acquired by overload exercise precede hypertrophy and are not lost on detraining. *Proceedings of the National Academy of Sciences*, 107(34), 15111-15116.

Bruusgaard, J.C., Egner, I.M., Larsen, T.K., Dupre-Aucouturier, S., Desplanches, D. and Gundersen, K., (2012). No change in myonuclear number during muscle unloading and reloading. *Journal of applied physiology*, 113(2), 290-296.

Camera, D.M., Burniston, J.G., Pogson, M.A., Smiles, W.J. and Hawley, J.A., (2017). Dynamic proteome profiling of individual proteins in human skeletal muscle after a high-fat diet and resistance exercise. *The FASEB Journal*, 31(12), 5478-5494.

Campbell, K.P., (1995). Three muscular dystrophies: loss of cytoskeleton-extracellular matrix linkage. *Cell*, 80(5), 675-679.

Campbell, W.W. and Leidy, H. J., (2007). Dietary protein and resistance training effects on muscle and body composition in older persons. *Journal of the American College of Nutrition*, 26(6), 696S-703S.

Chandel, N.S., Jasper, H., Ho, T.T. and Passegué, E., (2016). Metabolic regulation of stem cell function in tissue homeostasis and organismal ageing. *Nature Cell Biology*, 18(8), 823-832.

Cheema, N., Herbst, A., McKenzie, D. and Aiken, J.M., (2015). Apoptosis and necrosis mediate skeletal muscle fiber loss in age-induced mitochondrial enzymatic abnormalities. *Aging cell*, 14(6), 1085-1093.

Chomczynski, P. and Sacchi, N., (1987). Single-step method of RNA isolation by acid guanidinium thiocyanate-phenol-chloroform extraction. *Analytical biochemistry*, 162(1), 156-159.

Cobley, J.N., Ab Malik, Z., Morton, J.P., Close, G.L., Edwards, B.J. and Burniston, J.G., (2016). Age-and activity-related differences in the abundance of myosin essential and regulatory light chains in human muscle. *Proteomes*, 4(2), 15.

Clarkson, P.M., Devaney, J.M., Gordish-Dressman, H., Thompson, P.D., Hubal, M.J., Urso, M., Price, T.B., Angelopoulos, T.J., Gordon, P.M., Moyna, N.M. and Pescatello, L.S., (2005). ACTN3 genotype is associated with increases in muscle strength in response to resistance training in women. *Journal of Applied Physiology*, 99(1), 154-163.

Damas, F., Phillips, S., Vechin, F.C. and Ugrinowitsch, C., (2015). A review of resistance training-induced changes in skeletal muscle protein synthesis and their contribution to hypertrophy. *Sports medicine*, 45(6), 801-807.

Davalos, V., Blanco, S. and Esteller, M., (2018). SnapShot: Messenger RNA Modifications. *Cell*, 174(2), 498-498.

Doherty, T.J., Vandervoort, A.A., Taylor, A.W. and Brown, W.F., (1993). Effects of motor unit losses on strength in older men and women. *Journal of Applied Physiology*, 74(2), 868-874.

Dupont-Versteegden, E.E., Strotman, B.A., Gurley, C.M., Gaddy, D., Knox, M., Fluckey, J.D. and Peterson, C.A., (2006). Nuclear translocation of EndoG at the initiation of disuse muscle atrophy and apoptosis is specific to myonuclei. *American Journal of Physiology-Regulatory, Integrative and Comparative Physiology*, 291(6), 1730-1740.

Egner, I.M., Bruusgaard, J.C., Eftestøl, E. and Gundersen, K., (2013). A cellular memory mechanism aids overload hypertrophy in muscle long after an episodic exposure to anabolic steroids. *The Journal of physiology*, 591(24), 6221-6230.

Egner, I.M., Bruusgaard, J.C. and Gundersen, K., (2016). Satellite cell depletion prevents fiber hypertrophy in skeletal muscle. *Development*, 143(16), 2898-2906.

Espigat-Georger A, Dyachuk V, Chemin C, Emorine L, Merdes (2016) A. Nuclear alignment in myotubes requires centrosome proteins recruited by nesprin-1. *Journal of Cell Science*, 129, 4227-4237.

Fisher, A.G., Seaborne, R.A., Hughes, T.M., Gutteridge, A., Stewart, C., Coulson, J.M., Sharples, A.P. and Jarvis, J.C., (2017). Transcriptomic and epigenetic regulation of disuse atrophy and the return to activity in skeletal muscle. *The FASEB Journal*, 31(12), 5268-5282.

Fehrer, C. and Lepperdinger, G., (2005). Mesenchymal Stem Cell Aging. *Experimental Gerontology*, 40(12), 926-930.

Ferreira, R., Neuparth, M.J., Ascensão, A., Magalhães, J., Vitorino, R., Duarte, J.A. and Amado, F., (2006). Skeletal muscle atrophy increases cell proliferation in mice gastrocnemius during the first week of hindlimb suspension. *European Journal Of Applied Physiology*, 97(3), 340-346.

Franchi, M.V., Reeves, N.D. and Narici, M.V., (2017). Skeletal muscle remodeling in response to eccentric vs. concentric loading: morphological, molecular, and metabolic adaptations. *Frontiers In Physiology*, 8, 447.

Frontera, W.R., Hughes, V.A., Fielding, R.A., Fiatarone, M.A., Evans, W.J. and Roubenoff, R., (2000). Aging of skeletal muscle: a 12-yr longitudinal study. *Journal of applied physiology*, 88(4), 1321-1326.

Gimpel, P., Lee, Y.L., Sobota, R.M., Calvi, A., Koullourou, V., Patel, R., Mamchaoui, K., Nédélec, F., Shackleton, S., Schmoranzner, J. and Burke, B., (2017). Nesprin-1 α -dependent microtubule nucleation from the nuclear envelope via Akap450 Is necessary for nuclear positioning in muscle cells. *Current Biology*, 27(19), 2999-3009.

Gorgey, A.S. and Dudley, G.A., (2007). Skeletal muscle atrophy and increased intramuscular fat after incomplete spinal cord injury. *Spinal cord*, 45(4), 304.

Grobler, L., Collins, M. and Lambert, M.I., (2004). Remodelling of skeletal muscle following exercise-induced muscle damage. *International SportMed Journal*, 5(2), 67-83.

Gundersen, K., (2016). Muscle memory and a new cellular model for muscle atrophy and hypertrophy. *Journal of Experimental Biology*, 219(2), 235-242.

Guo, B.S., Cheung, K.K., Yeung, S.S., Zhang, B.T. and Yeung, E.W., (2012). Electrical stimulation influences satellite cell proliferation and apoptosis in unloading-induced muscle atrophy in mice. *PloS one*, 7(1), 30348.

Guzman-Castillo, M., Ahmadi-Abhari, S., Bandosz, P., Capewell, S., Steptoe, A., Singh Manoux, A., Kivimaki, M., Shipley, M.J., Brunner, E.J. and O'Flaherty, M., (2017). Forecasted trends in disability and life expectancy in England and Wales up to 2025: a modelling study. *The Lancet Public Health*, 2(7), 307-313.

Hawke, T.J. & Garry, D.J., (2001). Myogenic satellite cells: physiology to molecular biology. *Journal of Applied Physiology*, 91(2), 534-551.

Hesketh, S., Srisawat, K., Sutherland, H., Jarvis, J. and Burniston, J., (2016). On the rate of synthesis of individual proteins within and between different striated muscles of the rat. *Proteomes*, 4(1), 12.

Hill, M. and Goldspink, G. (2003a). Expression and Splicing of the Insulin-Like Growth Factor Gene in Rodent Muscle is Associated with Muscle Satellite (stem) Cell Activation following Local Tissue Damage. *The Journal of Physiology*, 549: 409–418.

Hill, M., Wernig, A. and Goldspink, G. (2003b). Muscle satellite (stem) cell activation during local tissue injury and repair. *Journal of Anatomy*, 203: 89–99.

Ho, K.W., Roy, R.R., Tweedle, C.D., Heusner, W.W., Van Huss, W.D. and Carrow, R.E., (1980). Skeletal muscle fiber splitting with weight-lifting exercise in rats. *American Journal of Anatomy*, 157(4), 433-440.

Hoppeler, H., (2016). Molecular networks in skeletal muscle plasticity. *Journal of Experimental Biology*, 219(2), 205-213.

Hornberger, T.A., Chu, W.K., Mak, Y.W., Hsiung, J.W., Huang, S.A. and Chien, S., (2006). The role of phospholipase D and phosphatidic acid in the mechanical activation of mTOR signaling in skeletal muscle. *Proceedings of the National Academy of Sciences*, 103(12), 4741-4746.

Hyldahl, R.D., Nelson, B., Xin, L., Welling, T., Groscost, L., Hubal, M.J., Chipkin, S., Clarkson, P.M. and Parcell, A.C., (2015). Extracellular matrix remodeling and its contribution to protective adaptation following lengthening contractions in human muscle. *The FASEB Journal*, 29(7), 2894-2904.

Inoki, K., Li, Y., Zhu, T., Wu, J. and Guan, K.L., (2002). TSC2 is phosphorylated and inhibited by Akt and suppresses mTOR signalling. *Nature cell biology*, 4(9), 648.

Jackaman, C., Nowak, K.J., Ravenscroft, G., Lim, E.M., Clément, S. and Laing, N.G., (2007). Novel application of flow cytometry: determination of muscle fiber types and protein levels in whole murine skeletal muscles and heart. *Cytoskeleton*, 64(12), 914-925.

Jackson, J.R., Mula, J., Kirby, T.J., Fry, C.S., Lee, J.D., Ubele, M.F., Campbell, K.S., McCarthy, J.J., Peterson, C.A. and Dupont-Versteegden, E.E., (2012). Satellite cell depletion does not inhibit adult skeletal muscle regrowth following unloading-induced atrophy. *American Journal of Physiology-Cell Physiology*, 303(8), 854-861.

Jacobs, B.L., You, J.S., Frey, J.W., Goodman, C.A., Gundermann, D.M. and Hornberger, T.A., (2013). Eccentric contractions increase the phosphorylation of tuberous sclerosis complex-2 (TSC2) and alter the targeting of TSC2 and the mechanistic target of rapamycin to the lysosome. *The Journal of Physiology*, 591(18), 4611-4620.

Jacobs, B.L., McNally, R.M., Kim, K.J., Blanco, R., Privett, R.E., You, J.S. and Hornberger, T.A., (2017). Identification of mechanically regulated phosphorylation sites on tuberin (TSC2) that control mechanistic target of rapamycin (mTOR) signaling. *Journal of Biological Chemistry*, M117.

Jakobsen, J.R., Jakobsen, N.R., Mackey, A.L., Koch, M., Kjaer, M. and Krogsgaard, M.R., (2018). Remodeling of muscle fibers approaching the human myotendinous junction. *Scandinavian journal of medicine & science in sports*.

Jarvis, J.C. and Salmons, S., (1991). A family of neuromuscular stimulators with optical transcutaneous control. *Journal of medical engineering & technology*, 15(2), 53-57.

Jarvis, J.C., Mokrusch, T., Kwende, M.M., Sutherland, H. and Salmons, S., (1996). Fast-to-slow transformation in stimulated rat muscle. *Muscle & Nerve: Official Journal of the American Association of Electrodiagnostic Medicine*, 19(11), 1469-1475

Johnston, A.P., De Lisio, M. and Parise, G., (2007). Resistance training, sarcopenia, and the mitochondrial theory of aging. *Applied physiology, nutrition, and metabolism*, 33(1), 191-199.

Jeevanandam, M., Lowry, S., Horowitz, G. and Brennan, M., (1984). Cancer cachexia and protein metabolism. *The Lancet*, 323(8392), 1423-1426.

Joubert, Y. and Tobin, C., (1995). Testosterone treatment results in quiescent satellite cells being activated and recruited into cell cycle in rat levator ani muscle. *Developmental Biology*, 169(1), 286-294.

Kadi, F. and Thornell, L.E., (2000). Concomitant increases in myonuclear and satellite cell content in female trapezius muscle following strength training. *Histochemistry and cell biology*, 113(2), 99-103.

Kadi, F., Charifi, N., Denis, C., Lexell, J., Andersen, J.L., Schjerling, P., Olsen, S. and Kjaer, M., (2005). The behaviour of satellite cells in response to exercise: what have we learned from human studies? *Pflügers Archiv*, 451(2), 319-327.

Kalyani, R.R., Corriere, M. and Ferrucci, L., (2014). Age-related and disease-related muscle loss: the effect of diabetes, obesity, and other diseases. *The Lancet Diabetes & Endocrinology*, 2(10), 819-829.

Kandarian, S.C., Young, J.C. and Gomez, E.E., (1992). Adaptation in synergistic muscles to soleus and plantaris muscle removal in the rat hindlimb. *Life sciences*, 51(21), 1691-1698.

Katta, A., Kakarla, S.K., Manne, N.D., Wu, M., Kundla, S., Kolli, M.B., Nalabotu, S.K. and Blough, E.R., (2012). Diminished muscle growth in the obese Zucker rat following overload is associated with hyperphosphorylation of AMPK and dsRNA-dependent protein kinase. *Journal of Applied Physiology*, 113(3), 377-384.

Kawano, F., Takeno, Y., Nakai, N., Higo, Y., Terada, M., Ohira, T., Nonaka, I. and Ohira, Y., (2008). Essential role of satellite cells in the growth of rat soleus muscle fibers. *American Journal of Physiology-Cell Physiology*, 295(2), 458-467.

Kelley, G., (1996). Mechanical overload and skeletal muscle fiber hyperplasia: a meta-analysis. *Journal of Applied Physiology*, 81(4), 1584-1588.

Knappe, S., Zammit, P.S. & Knight, R.D., (2015). A population of Pax7-expressing muscle progenitor cells show differential responses to muscle injury dependent on developmental stage and injury extent. *Frontiers in aging neuroscience*, 7.

Kramer, I.F., Snijders, T., Smeets, J.S., Leenders, M., van Kranenburg, J., den Hoed, M., Verdijk, L.B., Poeze, M. and van Loon, L.J., (2017). Extensive type II muscle fiber atrophy in elderly female hip fracture patients. *Journals of Gerontology Series A: Biomedical Sciences and Medical Sciences*, 72(10), 1369-1375.

Laemmli, U.K., (1970). Cleavage of structural proteins during the assembly of the head of bacteriophage T4. *Nature*, 227(5259), 680.

Lepper, C., Partridge, T.A. and Fan, C.M., (2011). An absolute requirement for Pax7-positive satellite cells in acute injury-induced skeletal muscle regeneration. *Development*, 138(17), 3639-3646.

Lexell, J., Taylor, C.C. and Sjöström, M., (1988). What is the cause of the ageing atrophy? Total number, size and proportion of different fiber types studied in whole vastus lateralis muscle from 15-to 83-year-old men. *Journal of the neurological sciences*, 84(2-3), 275-294.

Mackey, A.L., Magnan, M., Chazaud, B. and Kjaer, M., (2017). Human skeletal muscle fibroblasts stimulate in vitro myogenesis and in vivo muscle regeneration. *The Journal of Physiology*, 595(15), 5115–5127.

Mackey, A.L. and Kjaer, M., (2017). *The breaking and making of healthy adult human skeletal muscle in vivo*. *Skeletal Muscle*, 7(1), 24.

Maddaluno, L., Urwyler, C. and Werner, S., (2017). Fibroblast growth factors: key players in regeneration and tissue repair. *Development*, 144(22), 4047-4060.

McPhee, J.S., Cameron, J., Maden-Wilkinson, T., Piasecki, M., Yap, M.H., Jones, D.A. and Degens, H., (2018). The contributions of fibre atrophy, fibre loss, in situ specific force and voluntary activation to weakness in sarcopenia. *Journals of Gerontology, Series A*.

Meneses, C., Morales, M.G., Abrigo, J., Simon, F., Brandan, E. and Cabello-Verrugio, C., (2015). The angiotensin-(1–7)/Mas axis reduces myonuclear apoptosis during recovery from

angiotensin II-induced skeletal muscle atrophy in mice. *Pflügers Archiv-European Journal of Physiology*, 467(9), 1975-1984.

Miller, B.F., Konopka, A.R. and Hamilton, K.L., (2016). The rigorous study of exercise adaptations: why mRNA might not be enough. *Journal of Applied Physiology*, 121(2),594-596.

Miner, J.H. and Wold, B., (1990). Herculín, a fourth member of the MyoD family of myogenic regulatory genes. *Proceedings of the National Academy of Sciences*, 87(3), 1089-1093.

Morley, J.E., Argiles, J.M., Evans, W.J., Bhasin, S., Cella, D., Deutz, N.E., Doehner, W., & Fearon, K.C., (2010). Nutritional recommendations for the management of sarcopenia. *Journal of the American Medical Directors Association*, 11(6), 391-396.

Mounier, R., Lantier, L., Leclerc, J., Sotiropoulos, A., Pende, M., Daegelen, D., Sakamoto, K., Foretz, M. and Viollet, B., (2009). Important role for AMPK α 1 in limiting skeletal muscle cell hypertrophy. *The FASEB Journal*, 23(7), 2264-2273.

Murach, K.A., White, S.H., Wen, Y., Ho, A., Dupont-Versteegden, E.E., McCarthy, J.J. and Peterson, C.A., (2017). Differential requirement for satellite cells during overload-induced muscle hypertrophy in growing versus mature mice. *Skeletal muscle*, 7(1), 14.

Murach, K.A., Englund, D.A., Dupont-Versteegden, E.E., McCarthy, J.J. and Peterson, C.A., (2018). Myonuclear Domain Flexibility Challenges Rigid Assumptions on Satellite Cell Contribution to Skeletal Muscle Fiber Hypertrophy. *Frontiers in physiology*, 9.

Murach, K.A., Fry, C.S., Kirby, T.J., Jackson, J.R., Lee, J.D., White, S.H., Dupont-Versteegden, E.E., McCarthy, J.J. and Peterson, C.A., (2017). Starring or supporting role? Satellite cells and skeletal muscle fiber size regulation. *Physiology*, 33(1), 26-38.

Murphy, M.M., Lawson, J.A., Mathew, S.J., Hutcheson, D.A. and Kardon, G., (2011). Satellite cells, connective tissue fibroblasts and their interactions are crucial for muscle regeneration. *Development*, 138(17), 3625-3637.

Nederveen, J.P., Joannis, S., Snijders, T. and Parise, G., (2017). The Influence and Delivery of Cytokines and their Mediating Effect on Muscle Satellite Cells. *Current Stem Cell Reports*, 3(3), 192-201.

Nederveen, J.P., Snijders, T., Joannisse, S., Wavell, C.G., Mitchell, C.J., Johnston, L.M., Baker, S.K. and Phillips, S.M. (2017). Altered muscle satellite cell activation following 16 wk of resistance training in young men. *American Journal of Physiology-Regulatory, Integrative and Comparative Physiology*, 312(1), R85-R92.

Newman, A., 2013. *The art of detecting data and image manipulation*. Accessed online on the 29/08/2018 at www.elsevier.com/editors-update/story/publishing-ethics/the-art-of-detecting-data-and-image-manipulation.

Oishi, Y., Ogata, T., Yamamoto, K.I., Terada, M., Ohira, T., Ohira, Y., Taniguchi, K. and Roy, R.R., (2008). Cellular adaptations in soleus muscle during recovery after hindlimb unloading. *Acta Physiologica*, 192(3), 381-395.

Pelosi, L., Giacinti, C., Nardis, C., Borsellino, G., Rizzuto, E., Nicoletti, C., Wannenes, F., and Battistini, L., (2007). Local expression of IGF-1 accelerates muscle regeneration by rapidly modulating inflammatory cytokines and chemokines. *The FASEB Journal*, 21(7), 1393-1402.

Petrella, J.K., Kim, J.S., Cross, J.M., Kosek, D.J. and Bamman, M.M., (2006). Efficacy of myonuclear addition may explain differential myofiber growth among resistance-trained young and older men and women. *American Journal of Physiology-Endocrinology and Metabolism*, 291(5), 937-946.

Petrella, J.K., Kim, J.S., Mayhew, D.L., Cross, J.M. and Bamman, M.M., (2008). Potent myofiber hypertrophy during resistance training in humans is associated with satellite cell-mediated myonuclear addition: a cluster analysis. *Journal of applied physiology*, 104(6), 1736-1742.

Pette, D. and Staron, R.S., (2001). Transitions of muscle fiber phenotypic profiles. *Histochemistry and cell biology*, 115(5), 359-372.

Phillips, S.M., (2014). A brief review of critical processes in exercise-induced muscular hypertrophy. *Sports Medicine*, 44(1), 71-77.

Piasecki, M., Ireland, A., Piasecki, J., Stashuk, D.W., Swiecicka, A., Rutter, M.K., Jones, D.A. and McPhee, J.S., (2018). Failure to expand the motor unit size to compensate for declining motor unit numbers distinguishes sarcopenic from non-sarcopenic older men. *The Journal of physiology*, 596(9), 1627-1637.

Phillips, S.M. and McGlory, C., (2014). CrossTalk proposal: The dominant mechanism causing disuse muscle atrophy is decreased protein synthesis. *The Journal of physiology*, 592(24), 5341-5343.

Phillips, S.M. and McGlory, C., (2014). CrossTalk proposal: The dominant mechanism causing disuse muscle atrophy is decreased protein synthesis. *The Journal of physiology*, 592(24), 5341-5343.

Posthumus, M., September, A.V., O'Cuinneagain, D., van der Merwe, W., Schwellnus, M.P. and Collins, M., (2009). The COL5A1 gene is associated with increased risk of anterior cruciate ligament ruptures in female participants. *The American journal of sports medicine*, 37(11), 2234-2240.

Potts, G.K., McNally, R.M., Blanco, R., You, J.S., Hebert, A.S., Westphall, M.S., Coon, J.J. and Hornberger, T.A., (2017). A map of the phosphoproteomic alterations that occur after a bout of maximal-intensity contractions. *The Journal of physiology*, 595(15), 5209-5226.

Rennie, M.J., Edwards, R.H.T., Millward, D.J., Wolman, S.L., Halliday, D. and Matthews, D.E., (1982). Effects of Duchenne muscular dystrophy on muscle protein synthesis. *Nature*, 296(5853), 165.

Roth, S.M., Martel, G.F., Ivey, F.M., Lemmer, J.T., Tracy, B.L., Hurlbut, D.E., Metter, E.J., Hurley, B.F. & Rogers, M.A., (1999). Ultrastructural muscle damage in young vs. older men after high-volume, heavy-resistance strength training. *Journal of Applied Physiology*, 86(6), 1833-1840.

Roth, S.M., Martel, G.F., Ivey, F.M., Lemmer, J.T., Tracy, B.L., Metter, E.J., Hurley, B.F. and Rogers, M.A., (2001). Skeletal muscle satellite cell characteristics in young and older men and women after heavy resistance strength training. *The Journals of Gerontology Series A: Biological Sciences and Medical Sciences*, 56(6), 240-247.

Rudrappa, S.S., Wilkinson, D.J., Greenhaff, P.L., Smith, K., Idris, I. and Atherton, P.J., (2016). Human skeletal muscle disuse atrophy: effects on muscle protein synthesis, breakdown, and insulin resistance—a qualitative review. *Frontiers in physiology*, 7, 361.

Sabatini, D.M., Erdjument-Bromage, H., Lui, M., Tempst, P. and Snyder, S.H., (1994). RAFT1: a mammalian protein that binds to FKBP12 in a rapamycin-dependent fashion and is homologous to yeast TORs. *Cell*, 78(1), 35-43.

Salter, A.C.D., Richmond, F.J. and Loeb, G.E., (2003). Effects of muscle immobilization at different lengths on tetrodotoxin-induced disuse atrophy. *IEEE Transactions on neural systems and rehabilitation engineering*, 11(3), 209-217.

Abou Sawan, S., Vliet, S., Parel, J.T., Beals, J.W., Mazzulla, M., West, D.W., Philp, A., Li, Z., Paluska, S.A., Burd, N.A. and Moore, D.R., (2018). Translocation and protein complex co-localization of mTOR is associated with postprandial myofibrillar protein synthesis at rest and after endurance exercise. *Physiological reports*, 6(5).

Saxton, R.A. and Sabatini, D.M., (2017). mTOR signaling in growth, metabolism, and disease. *Cell*, 168(6), 960-976.

Schmoll, M., Unger, E., Sutherland, H., Haller, M., Bijak, M., Lanmüller, H. and Jarvis, J.C., (2017). In-situ measurements of tensile forces in the tibialis anterior tendon of the rat in concentric, isometric, and resisted co-contractions. *Physiological reports*, 5(8).

Seaborne, R.A., Strauss, J., Cocks, M., Shepherd, S., O'Brien, T.D., Someren, K.A., Bell, P.G., Murgatroyd, C., Morton, J.P., Stewart, C.E. and Sharples, A.P., (2018). Human Skeletal Muscle Possesses an Epigenetic Memory of Hypertrophy. *Scientific reports*, 8(1), 1898.

Sharples, A.P., Stewart, C.E. and Seaborne, R.A., (2016). Does skeletal muscle have an 'epi'-memory? The role of epigenetics in nutritional programming, metabolic disease, aging and exercise. *Aging cell*, 15(4), 603-616.

Sinha-Hikim, I., Roth, S.M., Lee, M.I. and Bhasin, S., (2003). Testosterone-induced muscle hypertrophy is associated with an increase in satellite cell number in healthy, young men. *American Journal of Physiology-Endocrinology and Metabolism*, 285(1), 197-205.

Siracusa, J., Koulmann, N., Sourdille, A., Bourdon, S., Goriot, M.E. and Banzet, S., (2018). Phenotype-specific response of circulating miRNAs provides new biomarkers of slow or fast muscle damage. *Frontiers in Physiology*, 9, 684.

Siu, P.M. and Alway, S.E., (2005). Mitochondria-associated apoptotic signalling in denervated rat skeletal muscle. *The Journal of physiology*, 565(1), 309-323.

Siu, P.M., Pistilli, E.E. and Alway, S.E., (2005). Apoptotic responses to hindlimb suspension in gastrocnemius muscles from young adult and aged rats. *American Journal of Physiology-Regulatory, Integrative and Comparative Physiology*, 289(4), 1015-1026.

Smith, K.L. and Tisdale, M.J., (1993). Increased protein degradation and decreased protein synthesis in skeletal muscle during cancer cachexia. *British journal of cancer*, 67(4), 680.

Song, Z., Moore, D.R., Hodson, N., Ward, C., Dent, J.R., O'leary, M.F., Shaw, A.M., Hamilton, D.L., Sarkar, S., Gangloff, Y.G. and Hornberger, T.A., (2017). Resistance exercise initiates mechanistic target of rapamycin (mTOR) translocation and protein complex co-localisation in human skeletal muscle. *Scientific Reports*, 7(1), 5028.

Sola, O.M., Christensen, D.L. and Martin, A.W., (1973). Hypertrophy and hyperplasia of adult chicken anterior latissimus dorsi muscles following stretch with and without denervation. *Experimental neurology*, 41(1), 76-100.

Soukup, T., Zachařová, G. and Smerdu, V., (2002). Fibre type composition of soleus and extensor digitorum longus muscles in normal female inbred Lewis rats. *Acta histochemica*, 104(4), 399-405.

Spendiff, S., Vuda, M., Gouspillou, G., Aare, S., Perez, A., Morais, J.A., Jagoe, R.T., Filion, M.E., Glicksman, R., Kapchinsky, S. and MacMillan, N.J., (2016). Denervation drives mitochondrial dysfunction in skeletal muscle of octogenarians. *The Journal of physiology*, 594(24), 7361-7379.

Srisawat, K., Shepherd, S.O., Lisboa, P.J. and Burniston, J.G., (2017). A Systematic Review and Meta-Analysis of Proteomics Literature on the Response of Human Skeletal Muscle to Obesity/Type 2 Diabetes Mellitus (T2DM) Versus Exercise Training. *Proteomes*, 5(4), 30.

Staron, R.S., Hagerman, F.C., Hikida, R.S., Murray, T.F., Hostler, D.P., Crill, M.T., Ragg, K.E. and Toma, K., (2000). Fiber type composition of the vastus lateralis muscle of young men and women. *Journal of histochemistry & cytochemistry*, 48(5), 623-629.

Strassburg, S., Springer, J. and Anker, S.D., (2005). Muscle wasting in cardiac cachexia. *The International Journal of Biochemistry & Cell Biology*, 37(10), 1938-1947.

Tamaki, T., Uchiyama, S. and Nakano, S.H.O.I.C.H.I., (1992). A weight-lifting exercise model for inducing hypertrophy in the hindlimb muscles of rats. *Medicine and science in sports and exercise*, 24(8), 881-886.

Tasić, D., Dimov, I., Petrović, V., Savić, T. and Dimov, D., (2011). Fiber Type Composition and Size of Fibers in the Rat Tibialis Anterior Muscle. *Acta Facultatis Medicae Naissensis*, 28(3).

Tidball, J.G., (2011). Mechanisms of muscle injury, repair, and regeneration. *Comprehensive Physiology*.

Teixeira, C.E. and Duarte, J.A., (2011). Myonuclear domain in skeletal muscle fibers. A critical review. *Archives of Exercise in Health and Disease*, 2(2), 92-101.

Thomas, D.R., (2007). Loss of skeletal muscle mass in aging: examining the relationship of starvation, sarcopenia and cachexia. *Clinical nutrition*, 26(4), 389-399.

Thomson, D.M., Fick, C.A. and Gordon, S.E., (2008). AMPK activation attenuates S6K1, 4E-BP1, and eEF2 signaling responses to high-frequency electrically stimulated skeletal muscle contractions. *Journal Of Applied Physiology*, 104(3), 625-632.

Verdijk, L.B., Gleeson, B.G., Jonkers, R.A., Meijer, K., Savelberg, H.H., Dendale, P. and van Loon, L.J., (2009). Skeletal muscle hypertrophy following resistance training is accompanied by a fiber type-specific increase in satellite cell content in elderly men. *Journals of Gerontology Series A: Biomedical Sciences and Medical Sciences*, 64(3), 332-339.

von Maltzahn, J., Jones, A.E., Parks, R.J. and Rudnicki, M.A., (2013). Pax7 is critical for the normal function of satellite cells in adult skeletal muscle. *Proceedings of the National Academy of Sciences*, 110(41), 16474-16479.

Vignali, D.A., (2000). Multiplexed particle-based flow cytometric assays. *Journal of immunological methods*, 243(1-2), 243-255.

Viguie, C.A., Lu, D.X., Huang, S.K., Rengen, H. and Carlson, B.M., (1997). Quantitative study of the effects of long-term denervation on the extensor digitorum longus muscle of the rat. *The Anatomical Record: An Official Publication of the American Association of Anatomists*, 248(3), 346-354.

Von Haehling, S., Ebner, N., Dos Santos, M.R., Springer, J. and Anker, S.D., (2017). Muscle wasting and cachexia in heart failure: mechanisms and therapies. *Nature Reviews Cardiology*, 14(6), 323.

Wackerhage, H. & Ratkevicius, A. (2008) Signal transduction pathways that regulate muscle growth. *Essays in Biochemistry*, 44, 99-108

Wackerhage, H. , (2014). *Molecular exercise physiology: an introduction*. Routledge.

Wada, K.I., Takahashi, H., Katsuta, S. and Soya, H., (2002). No decrease in myonuclear number after long-term denervation in mature mice. *American Journal of Physiology-Cell Physiology*, 283(2), 484-488.

Wall, B.T., Dirks, M.L., Snijders, T., van Dijk, J.W., Fritsch, M., Verdijk, L.B. and van Loon, L.J., (2015). Short-term muscle disuse lowers myofibrillar protein synthesis rates and induces anabolic resistance to protein ingestion. *American Journal of Physiology-Endocrinology and Metabolism*, 310(2), 137-147.

Wang, H., Listrat, A., Meunier, B., Gueugneau, M., Coudy-Gandilhon, C., Combaret, L., Taillandier, D., Polge, C., Attaix, D., Lethias, C. and Lee, K., (2014). Apoptosis in capillary endothelial cells in ageing skeletal muscle. *Aging Cell*, 13(2), 254-262.

Wilkerson, M.J., (2012). Principles and applications of flow cytometry and cell sorting in companion animal medicine. *Veterinary Clinics: Small Animal Practice*, 42(1), 53-71.

Wilkinson, D.J., Piasecki, M. and Atherton, P.J., (2018). The age-related loss of skeletal muscle mass and function: measurement and mechanisms of muscle fibre atrophy and muscle fibre loss in humans. *Ageing research reviews*.

Winje, I.M., Bengtsen, M., Eftestøl, E., Juvkam, I., Bruusgaard, J.C. and Gundersen, K., (2018). Specific labelling of myonuclei by an antibody against pericentriolar material 1 on skeletal muscle tissue sections. *Acta Physiologica*, 13034.

Yang, N., MacArthur, D.G., Gulbin, J.P., Hahn, A.G., Beggs, A.H., Easteal, S. and North, K., (2003). ACTN3 genotype is associated with human elite athletic performance. *The American Journal of Human Genetics*, 73(3), 627-631.

Yin, H., Price, F. and Rudnicki, M.A., (2013). Satellite cells and the muscle stem cell niche. *Physiological reviews*, 93(1), 23-67.

You, J.S., Lincoln, H.C., Kim, C.R., Frey, J.W., Goodman, C.A., Zhong, X.P. and Hornberger, T.A., (2014). The role of diacylglycerol kinase ζ and phosphatidic acid in the mechanical activation of mammalian target of rapamycin (mTOR) signaling and skeletal muscle hypertrophy. *Journal of Biological Chemistry*, 289(3), 1551-1563.

You, J.S., Dooley, M.S., Kim, C.R., Kim, E.J., Xu, W., Goodman, C.A. and Hornberger, T.A., (2018). A DGK ζ -FoxO-ubiquitin proteolytic axis controls fiber size during skeletal muscle remodeling. *Science Signaling*, 11(530), 6847.

Zammit, P.S., Golding, J.P., Nagata, Y., Hudon, V., Partridge, T.A. and Beauchamp, J.R., (2004). Muscle satellite cells adopt divergent fates. *Journal Cell Biology*, 166(3), 347-357.

Zhang, B.T., Yeung, S.S., Liu, Y., Wang, H.H., Wan, Y.M., Ling, S.K., Zhang, H.Y., Li, Y.H. and Yeung, E.W., (2010). The effects of low frequency electrical stimulation on satellite cell activity in rat skeletal muscle during hindlimb suspension. *BMC cell biology*, 11(1), 87.

Zhang, J., Kim, J., Alexander, A., Cai, S., Tripathi, D.N., Dere, R., Tee, A.R., Tait-Mulder, J., Di Nardo, A., Han, J.M. and Kwiatkowski, E., (2013). A tuberous sclerosis complex signaling node at the peroxisome regulates mTORC1 and autophagy in response to ROS. *Nature cell biology*, 15(10), 1186.

Zhu, S., Nagashima, M., Khan, M.A., Yasuhara, S., Kaneki, M. and Martyn, J.J., (2013). Lack of caspase-3 attenuates immobilization-induced muscle atrophy and loss of tension generation along with mitigation of apoptosis and inflammation. *Muscle & nerve*, 47(5), 711-721.

Zoppi, N., Gardella, R., De Paepe, A., Barlati, S. and Colombi, M., (2004). Human fibroblasts with mutations in COL5A1 and COL3A1 genes do not organize collagens and fibronectin in

the extracellular matrix, down-regulate $\alpha 2\beta 1$ integrin and recruit $\alpha v\beta 3$ instead of $\alpha 5\beta 1$ integrin.
Journal of Biological Chemistry.